nature immunology

ARTICLES

https://doi.org/10.1038/s41590-022-01313-z

Check for updates

Memory CD8+ T cell diversity and B cell responses correlate with protection against SARS-CoV-2 following mRNA vaccination

Nadia Brasu[1,2,12], Ines Elia[1,3,12], Valentina Russo[1,2,12], Gaia Montacchiesi[1,2,12], Simona Aversano Stabile[1,3,12], Carlo De Intinis[1,3], Francesco Fesi[3], Katiuscia Gizzi[1,3], Marco Macagno[3], Monica Montone[3], Benedetta Mussolin[3], Alba Grifoni[4], Silvia Faravelli[5], Silvia Marchese[6], Federico Forneris[5], Raffaele De Francesco[6,7], Alessandro Sette[4,8], Vincenzo Barnaba[9,10], Antonino Sottile[3], Anna Sapino[3,11,13] and Luigia Pace[1,3,13] ✉

Understanding immune responses to SARS-CoV-2 messenger RNA (mRNA) vaccines is of great interest, principally because of the poor knowledge about the mechanisms of protection. In the present study, we analyzed longitudinally B cell and T cell memory programs against the spike (S) protein derived from ancestral SARS-CoV-2 (Wuhan-1), B.1.351 (beta), B.1.617.2 (delta) and B.1.1.529 (omicron) variants of concern (VOCs) after immunization with an mRNA-based vaccine (Pfizer). According to the magnitude of humoral responses 3 months after the first dose, we identified high and low responders. Opposite to low responders, high responders were characterized by enhanced antibody-neutralizing activity, increased frequency of central memory T cells and durable S-specific CD8+ T cell responses. Reduced binding antibodies titers combined with long-term specific memory T cells that had distinct polyreactive properties were found associated with subsequent breakthrough with VOCs in low responders. These results have important implications for the design of new vaccines and new strategies for booster follow-up.

In the last 2 years, infection with the severe acute respiratory syndrome coronavirus 2 (SARS-CoV-2)[1] has caused remarkable morbidity and mortality. There are hopes that herd immunity, achieved through both natural SARS-CoV-2 infection and vaccination, can control it[2]. Memory B cells, CD4+ T cells and CD8+ T cells elicited by SARS-CoV-2 mRNA vaccination have a critical role in the protection against infection and represent key determinants in the vaccine boost[2]. Both Pfizer/BioNTech and Moderna mRNA vaccines show 91% and 93% protective immunity over 7 months[3–5], respectively, and up to 95% efficacy in preventing symptomatic COVID-19 disease caused by the wild-type (WT) SARS-CoV-2 and delta and omicron VOCs[6–8].

Analyses of SARS-CoV-2-infected individuals has indicated the activation of both B and T cells in some subjects, but also discordant results in others[9]. Although studies in Middle East respiratory syndrome and SARS-CoV-1 infections suggest the long persistence of T cells and their ability to confer protection[10,11], the extent to which vaccine-elicited CD4+ and CD8+ T cell immunity is a correlate of protection against SARS-CoV-2 and VOCs remains poorly understood. The contribution of T cell immunity may in fact be superior compared with antibody protection against divergent VOCs, such as omicron, which escape neutralizing antibodies, as reported in nonhuman primates[12]. Based on these considerations, understanding the mechanisms of protective B and T cell memory responses would allow the development of new vaccination protocols and follow-ups to monitor protection.

In the case of subjects infected with SARS-CoV-2, natural immunity has been reported to be 93–100% protective against symptomatic disease for at least 8 months[13–15]. As such, individuals resolving previous SARS-CoV-2 infection have been vaccinated within 12 months after infection to achieve long-term protection (hybrid immunity)[16–18]. Hybrid immunity elicits substantially higher amounts of cross-variant neutralizing antibodies compared with those elicited by the vaccination of naive donors[16–19]. This strong immunity may be linked to the higher clonal turnover of B cells and greater somatic hypermutation in SARS-CoV-2-recovered compared with naive vaccinated individuals[20,21]. Although several studies have reported the contribution of virus-specific B and T cells to the protective immunity or immunopathology in SARS-CoV-2-vaccinated, -recovered or -infected individuals[18,22–24], it is still unclear whether hybrid immunity generates a more robust repertoire of memory B and T cells when compared with immunity generated after vaccination.

The emergence of the new VOCs such as B.1.351 (beta), B.1.617.2 (delta) and B.1.1.529 (omicron) has brought some insight into the mechanisms of protection of the mRNA vaccines against these

[1]G. Armenise-Harvard Immune Regulation Unit, IIGM, Candiolo, TO, Italy. [2]Department of Oncology, University of Turin, Turin, Italy. [3]Candiolo Cancer Institute, FPO-IRCCS, Candiolo, TO, Italy. [4]Center for Infectious Disease and Vaccine Research, La Jolla Institute for Immunology, La Jolla, CA, USA. [5]Armenise-Harvard Lab. of Structural Biology Dept. Biology and Biotechnology, University of Pavia, Pavia, Italy. [6]Istituto Nazionale Genetica Molecolare 'Romeo ed Enrica Invernizzi', Milan, Italy. [7]Department of Pharmacological and Biomolecular Sciences, University of Milan, Milan, Italy. [8]Department of Medicine, Division of Infectious Diseases and Global Public Health, University of California San Diego, La Jolla, CA, USA. [9]Pasteur Institute Italy—Fondazione Cenci Bolognetti, Rome, Italy. [10]Departement Scienze Cliniche, Interistiche, Anestesiologiche e Cardiovascolari, Sapienza University, Rome, Italy. [11]Department of Medical Sciences, University of Turin, Turin, Italy. [12]These authors contributed equally: Nadia Brasu, Ines Elia, Valentina Russo. [13]These authors jointly supervised this work: Anna Sapino, Luigia Pace. ✉e-mail: luigia.pace@iigm.it

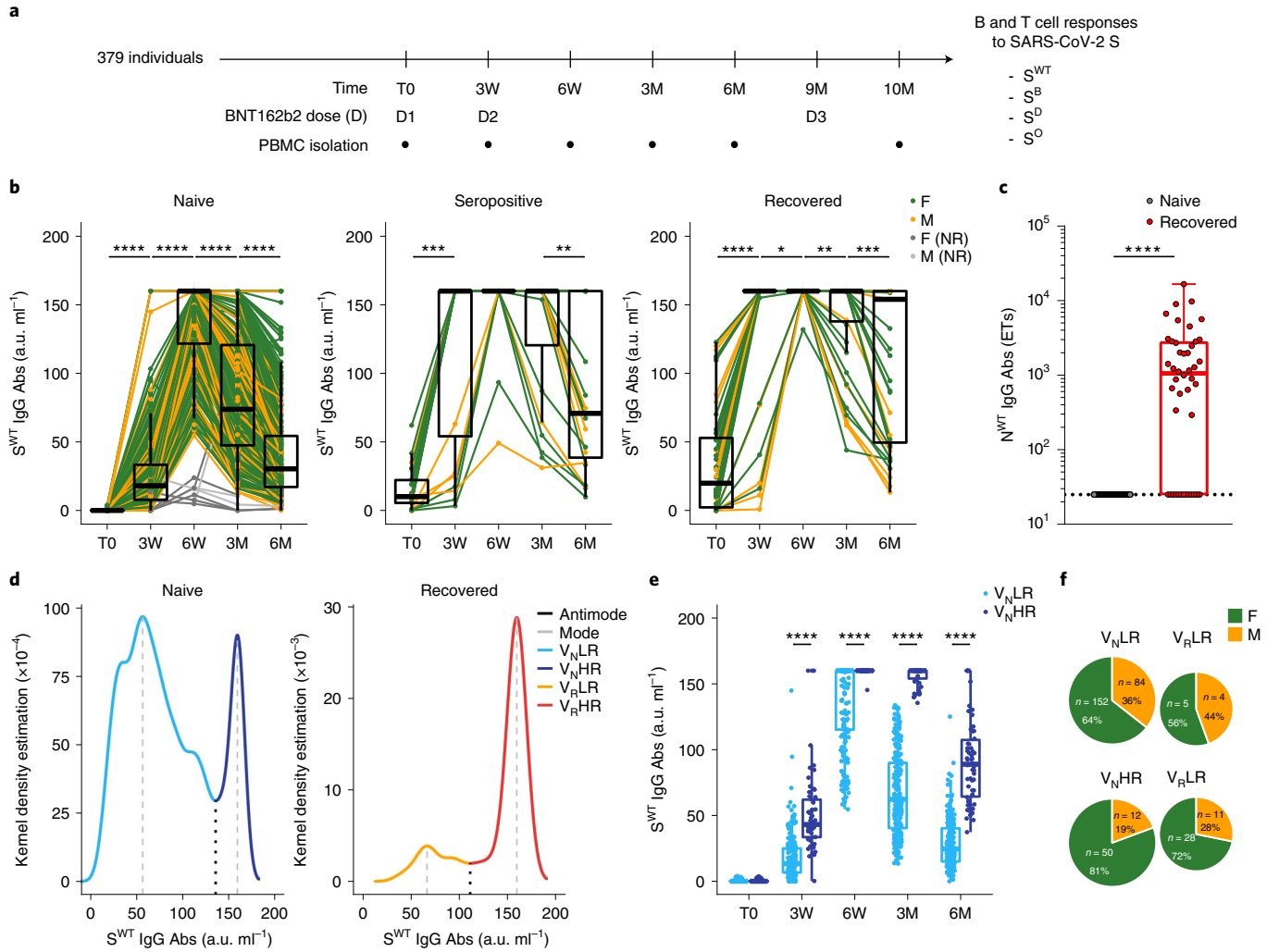

Fig. 1 | Longitudinal analysis of humoral responses to BNT162b2 mRNA vaccine. a, Experimental design of the study in which 379 individuals were vaccinated with the BNT162b2 mRNA vaccine and PBMCs were isolated before the administration of the first vaccine dose (T0), before the administration of the second vaccine dose at week 3 (3W), week 6 (6W), month 3 (3M) and month 6 (6M) and 1 month after the administration of the third vaccine dose, corresponding to month 10 (10M) after the first vaccine dose, followed by the analysis of humoral and T cell responses against the SARS-CoV-2 spike (S) proteins corresponding to the wild type (S^{WT}), beta (S^{B}), delta (S^{D}) and omicron (S^{O}) variants. **b**, Time series plots of S^{WT} IgG titers measured in SARS-CoV-2-naive, seropositive and SARS-CoV-2-recovered subjects. Abs, antibodies; a.u., arbitrary units; F, female; M, male, NR, nonresponder. Upper LOD = 160 a.u. ml^{-1}. **c**, ELISA of N^{WT} antibody titers in naive ($n = 307$) and recovered ($n = 48$) subjects measured before vaccination (T0). All data are shown as ELISA endpoint titers (ETs) based on a standard. The dotted line indicates the LOD. **d**, Kernel density estimation for S^{WT} IgG titer distribution at 3M after two vaccine doses in vaccinated naive high and low responders (V_NHRs and V_NLRs; left) and in vaccinated recovered high and low responders (V_RHRs and V_RLRs; right). The curves are composed of 32,768 points with a distance between adjacent points of 5.82×10^{-3} a.u. ml^{-1}. The total area under the density curve ($A = 1$) is estimated through the Riemann sum with a normalizing constant of 0.999801. **e**, Box plots of S^{WT} IgG titers in V_NLRs and V_NHRs at T0, 3W, 6W, 3M and 6M. **f**, Pie charts of V_NLRs, V_NHRs, V_RLRs and V_RHRs at month 3 postvaccination, with annotations for number and percentage of females and males. Statistics were calculated using two-sided Wilcoxon's rank-sum test (**c** and **e**) or signed-rank test (**b**), with Benjamini–Hochberg correction for multiple testing. $^{*}P \leq 0.05$; $^{**}P \leq 0.01$; $^{***}P \leq 0.001$; $^{****}P \leq 0.0001$. The boxes show median, upper and lower quartiles and the whiskers show 1.5× the interquartile range (IQR) on either side (**b** and **e**) or minimum/maximum (**c**). Each dot represents one subject and the data are pooled.

mutants and the quality and persistence of cross-reactive memory T cells[2,25–28]. However, although long-term memory B cell and CD4+ T cell responses to vaccination against SARS-CoV-2 start to be elucidated[8,29,30], the diversification of CD4+ and CD8+ T cells is not completely understood. This is particularly relevant for delta and omicron, which can evade antibody responses and have been correlated with lower vaccine efficacy against COVID-19 symptoms[31,32], although only a minimal number of spike-specific major histocompatibility complex I epitopes are muted compared with WT S (S^{WT})[33].

In the present study, we analyzed the S-specific antibody durability in correlation with memory B cells, CD4+ T cells and CD8+ T cells in SARS-CoV-2-vaccinated naive (V_N) and SARS-CoV-2-vaccinated COVID-19-recovered (V_R) individuals. Based on B cell responses and distinct polyreactivity of memory CD4+ and CD8+ T cells, V_N and V_R individuals could be classified as high responders (HRs) and low responders (LRs). Responses in V_NHRs were mainly characterized by increased frequencies of S-specific $CCR7^{+}CD27^{+}CD45RA^{-}CD4^{+}$ central memory 1 T (T_{CM1}) cells and $CCR7^{+}CD27^{+}CD45RA^{-}CD8^{+}$ T_{CM1} cells when compared with V_NLRs. Responses in V_NHRs resembled those of V_R individuals, whereas V_NLRs were characterized by the accumulation of effector memory 2 T (T_{EM2}) cells. These distinct immune responses

correlated with protection against COVID-19 caused by infection with delta and omicron in V_NHRs and V_RHRs.

Results

Distinct S^{WT} antibody titers in V_N and V_R subjects after vaccination. We longitudinally examined a cohort of 379 healthcare workers (69% females, Candiolo Cancer Institute (CCI), a certified COVID-free hospital) who were vaccinated with three doses of the BNT162b2 mRNA vaccine encoding the S^{WT} (ref. [7]) at time 0 (T0, first dose), week 3 (second dose) and month 9 after the first dose (third dose) (Fig. 1a and Supplementary Table 1). Based on the results of previous SARS-CoV-2 mRNA PCR tests, COVID-19 diagnosis and antibody titers against the S^{WT} and nucleocapsid (N^{WT}) subjects were classified as: SARS-CoV-2 naive (N), no history of infection, negative mRNA PCR swabs throughout all tests (for testing protocols, see Methods) and negative antibody responses to S^{WT} and N^{WT} ($n=307$, 67% females); seropositive, no history of infection based on negative mRNA PCR tests, but low titers of antibodies specific to S^{WT} and/or N^{WT} ($n=24$, 79% females); and recovered (R), with a past infection event documented by positive SARS-CoV-2 mRNA PCR swabs and mild COVID-19 symptoms ($n=48$, 70% females) (Fig. 1b,c and Extended Data Fig. 1a,b). Peripheral blood was collected a few hours before the administration of the first vaccine dose (T0), and week 3, week 6, month 3, month 6 and month 10 postvaccination.

Based on the S^{WT}-specific immunoglobulin (Ig)M and IgG titers in plasma during the first 6 months postvaccination, 10 (of the 379, 67% females) participants did not respond to the vaccine (Fig. 1b and Extended Data Fig. 1b). At each time point, the median of S^{WT}-specific IgM titers was not significantly different between V_N and V_R subjects (Extended Data Fig. 1b). In contrast, V_R subjects had higher baseline and a delayed decrease in S^{WT}-specific IgG concentration compared with V_N subjects at all timepoints (Fig. 1b). In particular, S^{WT}-specific IgG amounts significantly increased compared with T0 at weeks 3 and 6 postvaccination and gradually decreased at months 3 and 6 in V_N subjects, whereas they remained high at month 3 and decreased at month 6 in V_R subjects, although less dramatically than in V_N subjects (Fig. 1b). After a peak between weeks 1 and 3, the S^{WT}-specific IgG titers declined between months 3 and 6 in V_N subjects (Fig. 1b). At month 3 postvaccination, the Kernel density estimation of S^{WT}-specific IgG titers showed a bimodal distribution in V_N subjects (Fig. 1d). Based on the antimode value (that is, the least frequent value between the modes, cut-off 135 a.u. ml^{-1}), the 298 V_N subjects were divided into V_NLRs ($n=236$, 64% females) and V_NHRs ($n=62$, 81% females) (Fig. 1e). Similarly, based on the antimode value (112 a.u. ml^{-1}), the V_R cohort was classified as V_RHRs ($n=39$, 72% females) and V_RLRs ($n=9$, 56% females) (Fig. 1d and Extended Data Fig. 1c). Both V_NHRs and V_NLRs were negative for N^{WT}-specific IgGs (Fig. 1c). Of note, at month 3 postvaccination, there was increased frequency of females among V_NHRs (81%) compared with LRs (64%, Fisher's test $P=0.01481$; Fig. 1f). No correlation was found between age and S^{WT}-specific IgG titers at month 6 postvaccination (Extended Data Fig. 1d), although S^{WT}-specific IgG titers were significantly higher in the 20- to 29-year-old group than in all the others (Extended Data Fig. 1e). These results indicated durable S^{WT}-specific IgG responses in all cohorts, with higher titers in V_R than V_N subjects, and distinguished V_NHRs and V_NLRs based on the bimodal distribution of S^{WT}-specific IgG titers.

mRNA vaccine induces B cell responses and RBD antibodies. To determine whether the S^{WT}-specific IgG titers correlated with B cell frequencies, peripheral blood mononuclear cells (PBMCs) collected at T0, week 6 and month 6 postvaccination were stained with SARS-CoV-2 S^{WT} tetramers in the presence of antibodies for CD19, CD27, IgG, IgA and IgM (Fig. 2a and Extended Data Fig. 2a). No difference emerged in terms of the percentage of $CD19^+$ B cells at all timepoints tested (Extended Data Fig. 2b). Lower percentages of S^{WT}-specific B cells were found in V_NLRs and V_NHRs compared with V_R subjects at T0 and week 6 postvaccination (Fig. 2b and Extended Data Fig. 2a,c), but the frequency of S^{WT}-specific B cells increased significantly in V_NHRs compared with V_NLRs at month 6 postvaccination (Fig. 2b). The S^{WT}-specific IgG titers correlated with the frequency of S^{WT}-specific $tetramer^+$ B cells at month 6 in V_NHRs and V_R subjects (Fig. 2c). The frequency of S^{WT}-specific $tetramer^+$ B cells and $CD27^+$ IgG^+ B cells were higher in V_R subjects than in both V_NLRs and V_NHRs, especially at week 6 postvaccination (Fig. 2b,d). However, at month 6, the frequencies of S^{WT}-specific B cells and $CD27^+$ IgG^+ B cells equalized in V_R subjects and V_NHRs, whereas the frequency of S^{WT}-specific B cells and the numbers of $CD27^+IgG^+$ B cells remained significantly lower in V_NLRs than in the other two cohorts (Fig. 2b,d). The frequencies of S^{WT}-specific $CD27^+IgM^+$ B cells decreased in V_NHRs and V_NLRs (Extended Data Fig. 2d), whereas the frequency and numbers of S^{WT}-specific $CD27^+IgA^+$ B cells increased (Fig. 2e and Extended Data Fig. 2e) at month 6 postvaccination.

Next we measured the antibody titers against S^{WT} receptor-binding domain (RBD^{WT}) in the plasma collected from 30 V_NHRs, 30 V_NLRs and 26 V_R subjects at T0, month 3 and month 6 (Fig. 3a and Extended Data Fig. 3a). Although RBD^{WT}-specific antibodies were not detected in V_NHRs and V_NLRs at T0, robust RBD^{WT}-specific antibody titers were detected in V_NHRs and V_R subjects compared with V_NLRs at month 6 postvaccination (Fig. 3a). A similar range of percentage values was detected for delta RBD (RBD^D) IgGs, whereas omicron RBD (RBD^O) crossbinding IgG titers were reduced in both V_NHRs and V_R subjects at months 3 and 6 (Fig. 3a). The RBD^D and RBD^O antibody titers were always lower in V_NLRs than in the other 2 cohorts at months 3 and 6 postvaccination (Fig. 3a).

To quantify the corresponding neutralizing capacity of S RBD-specific antibodies, we generated pseudotype viruses encoding S-RBD^{WT}, -RBD^D and -RBD^O. At month 6, V_NLRs had reduced ancestral pseudovirus-neutralizing responses compared with V_NHRs, with minimal activity against delta and complete absence of neutralization against omicron particles (Fig. 3b), and the reduced neutralization against the ancestral pseudoviruses in V_NLRs correlated with the reduced RBD^{WT} antibody titers (Fig. 3c). Overall, these results indicated poor crossbinding of RBD-specific antibodies in V_NLRs against delta and omicron variants, with almost complete lack of neutralizing activity 6 months postvaccination.

T cell polyreactivity varies among V_NLRs, V_NHRs and V_R subjects. To determine the polyreactivity of memory T cell responses against S^{WT}, S^D, S^O and beta S (S^B), PBMCs were stimulated for 24 h with peptide megapools spanning the aforementioned proteins, whereas PBMC cultures in medium or with interleukin (IL)-2 and CD3 plus CD28 antibodies were used as negative (background) or positive controls, respectively. To measure the $CD4^+$ and $CD8^+$ T cell responses elicited by vaccination, we quantified the frequency of $CD25^+CD69^+$ T cells in the PBMCs from 25 V_NLRs, 24 V_NHRs and 12 V_R subjects 24 h poststimulation and after background subtraction (as the percentage of $CD25^+CD69^+$ T cells measured in the paired PBMCs cultured in medium) at T0 and month 6 postvaccination (Fig. 4a and Extended Data Fig. 4a–c). No difference was observed in terms of percentages of total $CD4^+$ and $CD8^+$ T cells before stimulation (Extended Data Fig. 4d,e) and background activation (Extended Data Fig. 4f,g) in all three cohorts. The percentages of polyspecific $CD4^+$ T cells to both S^{WT} and S^B peptide megapools were significantly higher in V_R subjects than in V_NHRs and V_NLRs at T0 (Fig. 4b and Extended Data Fig. 4f). The percentage of $CD25^+CD69^+CD4^+$ T cells significantly increased on stimulation with S-peptide megapools in both V_NHRs and V_NLRs at month 6 compared with T0 (Fig. 4b and Extended Data Fig. 5a). Similar

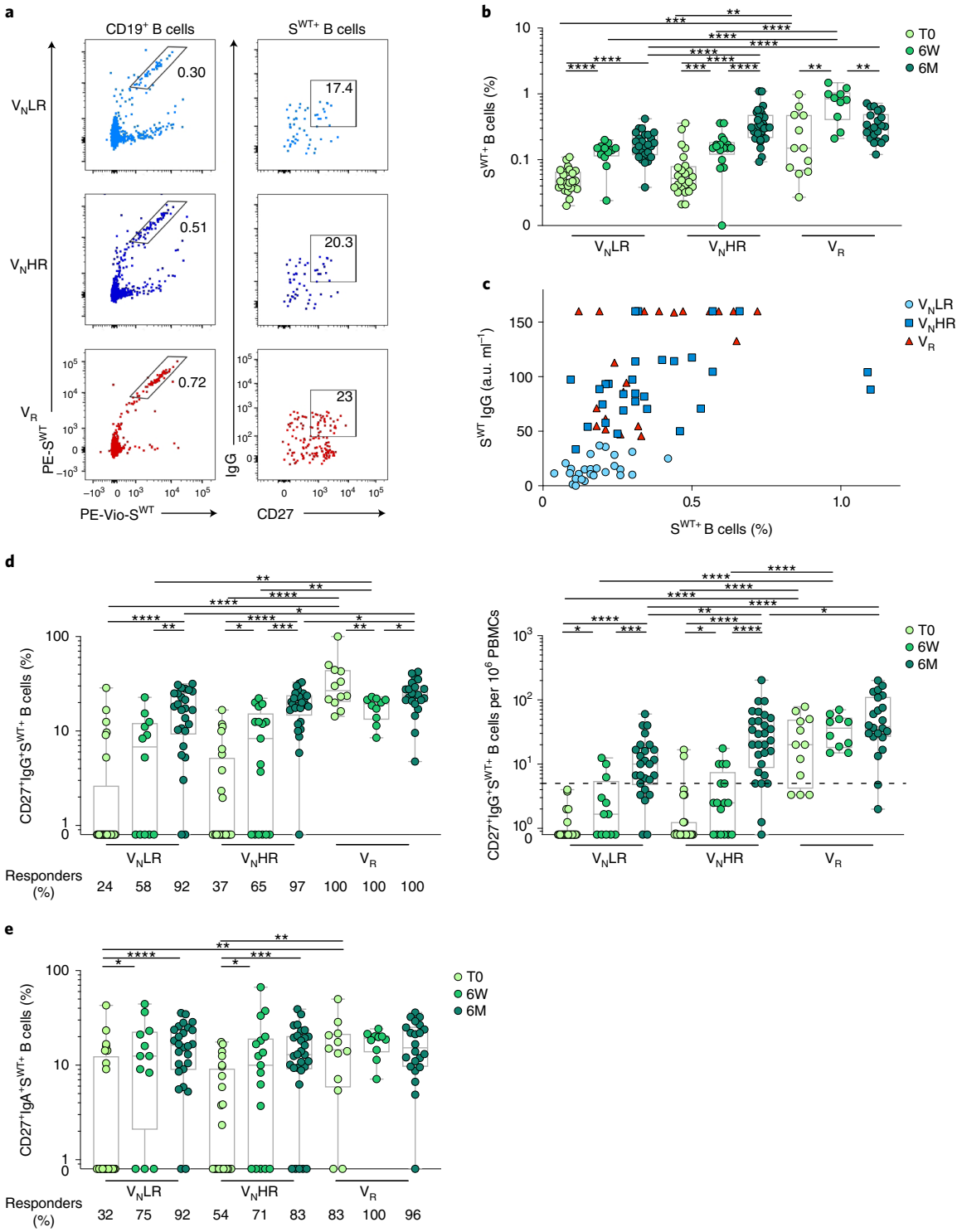

Fig. 2 | Dynamics of memory B cell responses after BNT162b2 mRNA vaccination. a, Representative flow cytometry dot plots of S^{WT}-tetramer$^+$ cells on gated CD19$^+$ B cells and of CD27$^+$ IgG$^+$ cells on gated S^{WT}-tetramer$^+$ B cells from V_NLR, V_NHR and V_R subjects at month 6. **b**, Flow cytometry analysis showing the percentage of S^{WT}-tetramer$^+$ B cells in V_NLR, V_NHR and V_R subjects at T0, week 6 and month 6. **c**, Spearman's correlation plot between S^{WT} IgG titers and percentage of S^{WT}-tetramer$^+$ B cells in V_NLR, V_NHR and V_R subjects at month 6 measured by flow cytometry; V_NLRs: $R = 0.388$ and $P =$ NS (not significant); V_NHRs: $R = 0.4471$ and $P < 0.05$; V_R subjects: $R = 0.4384$ and $P < 0.05$. **d**,**e**, Flow cytometry analysis showing the percentage and number per 10^6 PBMCs of CD27$^+$IgG$^+S^{WT+}$ B cells (**d**) and the percentage of CD27$^+$IgA$^+S^{WT+}$ B cells (**e**) in V_NLR, V_NHR and V_R subjects at T0, week 6 and month 6. Below: percentages of subjects with active responses > 0.01. The dashed black line shows the LOD. The same subjects were analyzed longitudinally at T0: V_NLRs ($n = 25$), V_NHRs ($n = 24$), V_R subjects ($n = 12$); 6 W: V_NLRs ($n = 12$), V_NHRs ($n = 17$), V_R subjects ($n = 10$); and 6 M: V_NLRs ($n = 26$), V_NHRs ($n = 29$), V_NR subjects ($n = 22$). The box plots indicate median, IQR and minimum/maximum. Each dot of the box plots represents the average across three technical replicates of the same subject; the data are pooled from multiple experiments. Statistics were calculated using two-sided Wilcoxon's rank-sum test. $^*P < 0.05$; $^{**}P < 0.01$; $^{***}P < 0.001$; $^{****}P < 0.0001$.

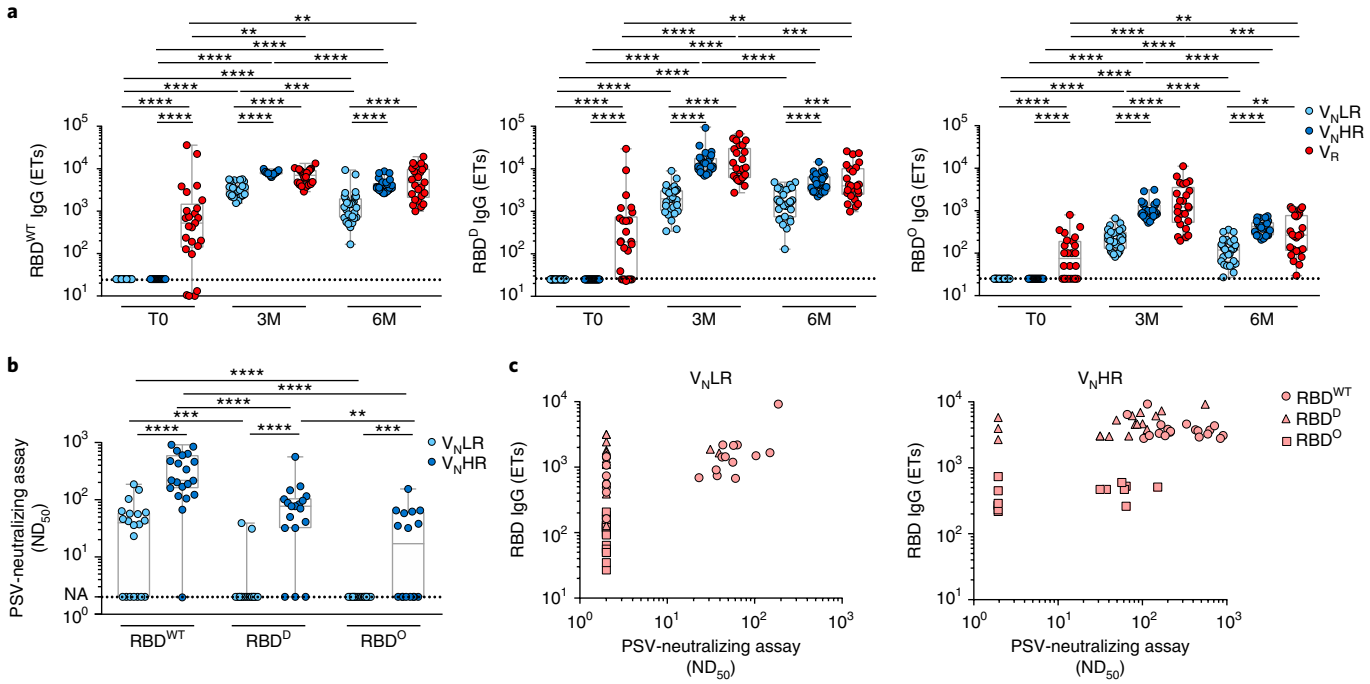

Fig. 3 | Anti-RBD-binding antibodies and neutralizing activity against ancestral and VOCs-derived spike. a, ELISA showing SARS-CoV-2 S-RBD^{WT}, -RBD^{D} and -RBD^{O} IgG titers in V_NLRs, V_NHRs and V_R subjects in plasma at T0, 3M and 6M. ELISA results shown as ETs based on a standard. The dotted lines represent the LOD. At T0: V_NLRs ($n=30$), V_NHRs ($n=30$), V_R subjects ($n=26$); 3M: V_NLRs ($n=28$), V_NHRs ($n=27$), V_R subjects ($n=25$); 6M: V_NLRs ($n=30$), V_NHRs ($n=29$), V_R subjects ($n=26$). **b**, Neutralization assay showing 50%neutralizing dose titers (ND_{50}) against S-RBD^{WT}, -RBD^{D} and -RBD^{O} measured by pseudovirus (PSV)-neutralizing assay in plasma from V_NLRs ($n=20$) and V_NHRs ($n=20$) at month 6. **c**, Spearman's correlation plots showing PSV ND_{50} and IgG ELISA ETs against S-RBD^{WT}, -RBD^{D} and -RBD^{O} in plasma from V_NLRs ($n=20$) and V_NHRs ($n=20$) at month 6. V_NLRs, RBD^{WT}: $R=0.721$ and $P<0.001$, RBD^{D}: $R=0.2305$ and $P=$NS, RBD^{O}: $P=$NS; V_NHRs, RBD^{WT}: $R=0.2168$ and $P=$NS, RBD^{D}: $R=0.6282$ and $P<0.01$, RBD^{O}: $R=0.4277$ and $P<0.01$. NA indicates no neutralizing activity. The same subjects were longitudinally analyzed. The box plots indicate median, IQR and minimum/maximum. Each dot of box plots represents the average across two (**a**) and three (**b**) technical replicates of the same subject; the data are pooled from multiple experiments. Statistics were calculated using two-sided Wilcoxon's signed-rank and two-sided Wilcoxon's rank-sum test. $^{**}P<0.01$; $^{***}P<0.001$; $^{****}P<0.0001$.

observations were made for CD25$^+$CD69$^+$CD8$^+$ T cell responses to the S^{WT}, S^{D} and S^{O} (Fig. 4c and Extended Data Figs. 4g and 5b). No differences were observed in terms of activation with the positive controls in all examined conditions (Extended Data Fig. 5c,d). Stimulation with S^{WT}, S^{D} and S^{O} peptide megapools elicited a consistent increase in the percentage of CD25$^+$CD69$^+$CD8$^+$ T cells in both V_NHRs and V_NLRs at month 6 postvaccination (Fig. 4c and Extended Data Fig. 5b).

We next assessed the effector T cell activity by investigating the expression of granzyme B and the effector cytokines interferon (IFN)-γ, tumor necrosis factor (TNF)-α and IL-2 after 14 h of stimulation of PBMCs isolated at T0 and month 6 with S-peptide megapools derived from WT, delta, omicron and beta variants, using PBMCs cultured with IL-2 and CD3 plus CD28 antibodies or medium as positive or negative controls, respectively (Extended Data Fig. 6a). There were no differences in the percentage of granzyme B$^+$ cells between T0 and month 6 in both V_NLR and V_NHR subjects (data not shown), whereas IFN-γ expression was elicited by all S-derived megapools in antigen-specific CD4$^+$ T cells and CD8$^+$ T cells, although at different levels, at month 6 (Fig. 4d). A significant increase in the T cell responses to S^{O} peptides was observed in V_NHRs and V_R subjects compared with V_NLRs (Fig. 4d), indicating a higher frequency of polyreactive T cells in those samples. By contrast, the percentages of IL-2$^+$ (Extended Data Fig. 6b) and TNF-α$^+$CD4$^+$ or -CD8$^+$ T cells (Extended Data Fig. 6c) were quite similar across all cohorts, as well as in the PBMCs stimulated with IL-2 and CD3 plus CD28 antibodies (positive controls; Extended Data Fig. 6d). These results showed that polyreactive, S-specific memory CD4$^+$ and CD8$^+$ T cell responses could be detected until month 6 postvaccination and that the frequencies of IFN-γ$^+$CD4$^+$ T cells or IFN-γ$^+$CD8$^+$ T cells reactive against S^{O} were reduced in V_NLRs compared with V_NHRs and V_R individuals.

Fig. 4 | Analysis of specific CD4$^+$ and CD8$^+$ T cell responses against S^{WT}, S^{D}, S^{O} and S^{B} in V_NLRs, V_NHRs and V_R subjects. a, Representative flow cytometry dot plots of CD25 versus (vs) CD69 cells on gated CD4$^+$ (left) and CD8$^+$ (right) T cells from V_NLRs, V_NHRs and V_R subjects at month 6, after 24h incubation with medium (Unstimulated) or S^{WT} peptide megapools. **b**,**c**, Flow cytometry analysis showing the percentage of CD25$^+$CD69$^+$ cells in CD4$^+$ T cells (**b**) and CD8$^+$ T cells (**c**) from V_NLRs, V_NHRs and V_R subjects at T0 and 6M, 24h after incubation with S^{WT}, S^{D}, S^{O} or S^{B}. Below: percentages of subjects with active responses >0.01. **d**, Flow cytometry analysis showing the percentage of IFN-γ$^+$ cells in CD4$^+$ T cells and CD8$^+$ T cells from V_NLRs, V_NHRs and V_R subjects at month 6, after 14h incubation with S^{WT}, S^{D}, S^{O} or S^{B}. Below: percentages of subjects with active responses >0.01. Data are represented with background subtraction from paired unstimulated controls. The same subjects were analyzed longitudinally at T0 and 6M: V_NLRs (n = 25), V_NHRs (n = 24) and V_R subjects (n = 12) . The box plots indicate median, IQR and minimum/maximum. Each dot of the box plots represents the average across three technical replicates of the same subject; the data are pooled from multiple experiments. Statistics were calculated using two-sided Wilcoxon's signed-rank and two-sided Wilcoxon's rank-sum test. $^{*}P<0.05$; $^{**}P<0.01$; $^{***}P<0.001$; $^{****}P<0.0001$.

Distinct memory T cell subsets react against S^{WT} and S^{o}. Several subsets of CD4+ and CD8+ T cells, such as CCR7+CD45RA− T_{CM} cells, CCR7−CD27+CD45RA- T_{EM1} cells, CCR7−CD27-CD45RA- T_{EM2} cells and terminally differentiated effector memory CD45RA+ T cells (T_{EMRA} cells) have been described[34–37]. Based on immune phenotype, transcriptional and epigenetic programs, CD8+ T_{EM1} cells

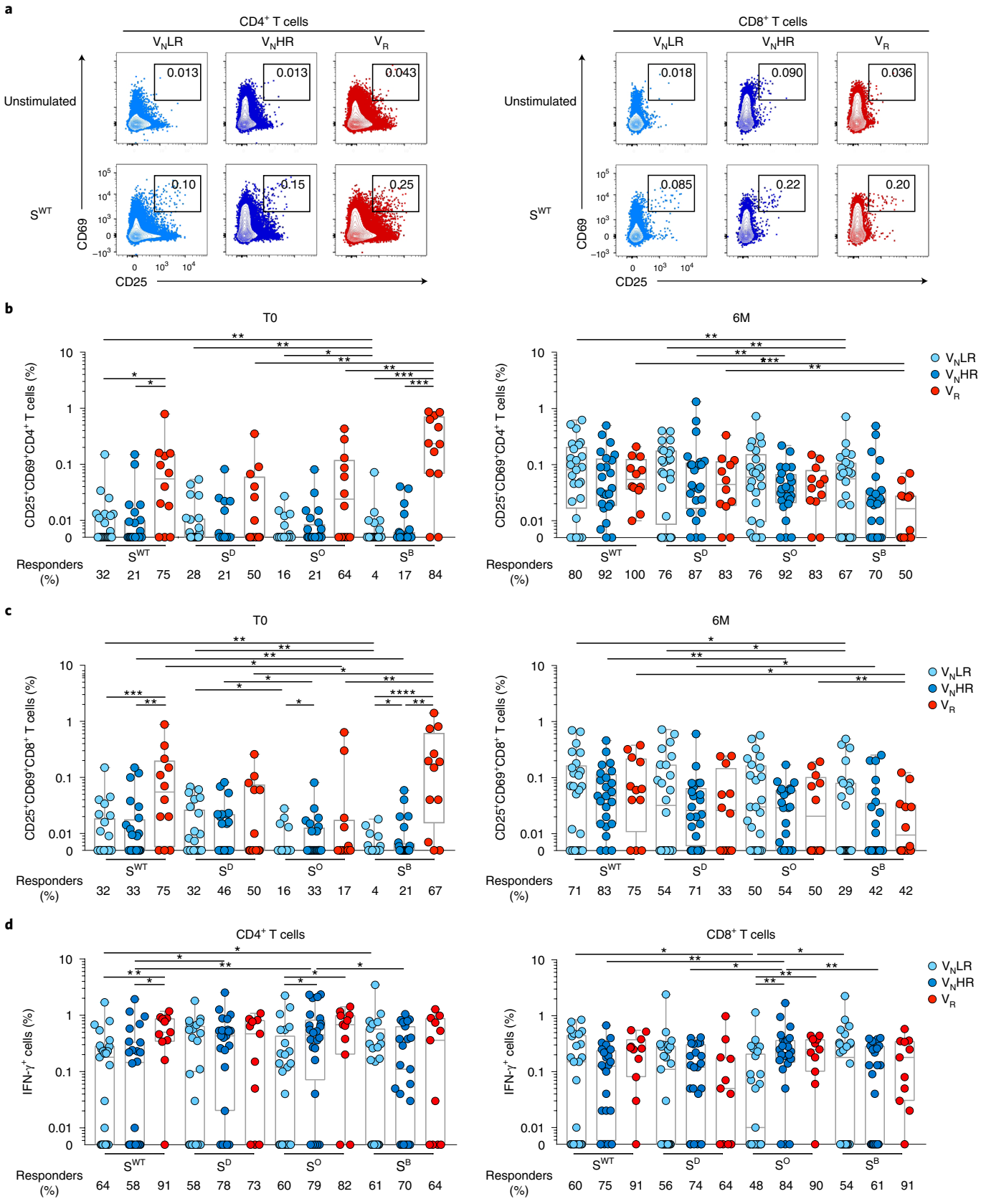

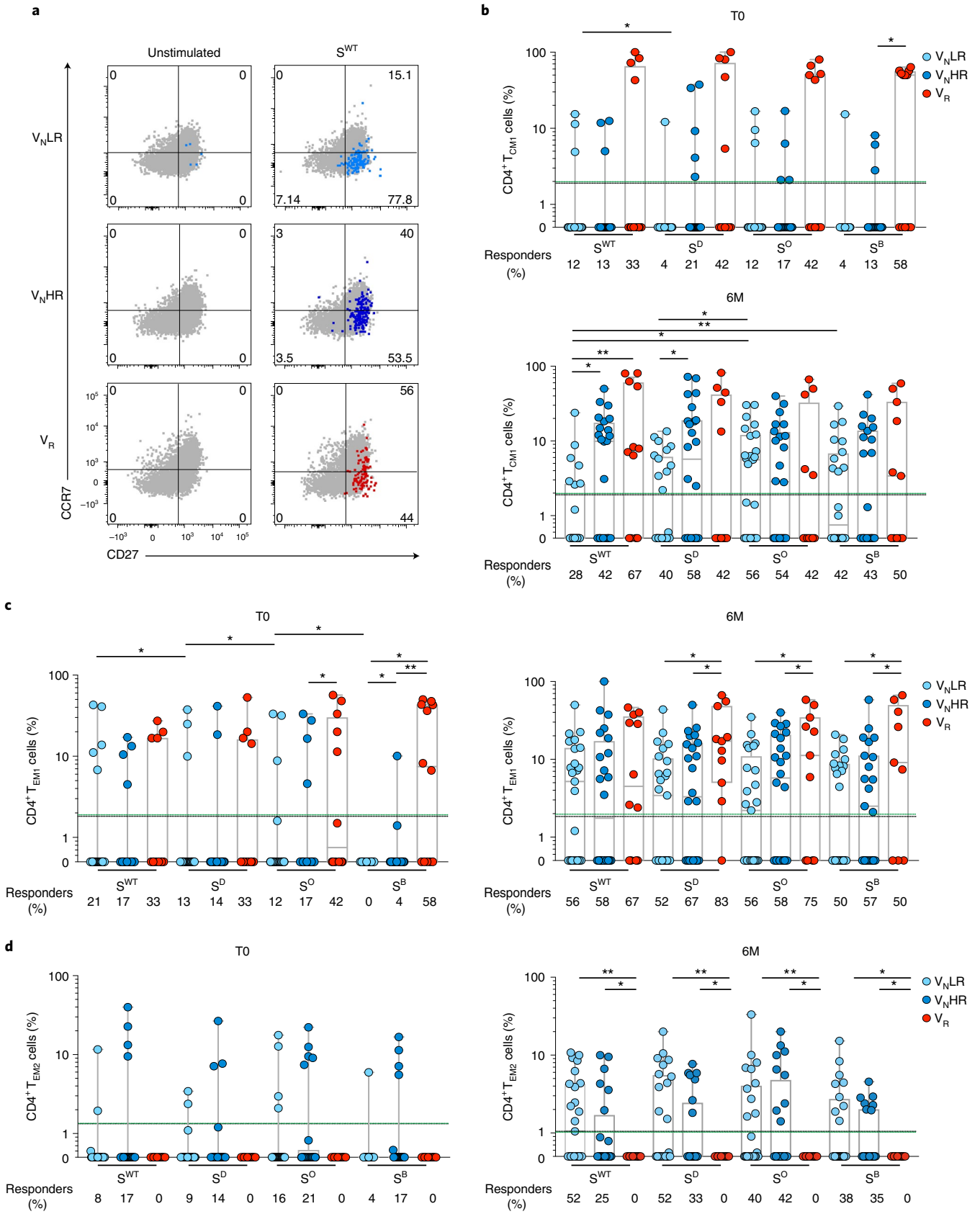

are closely related to CD8⁺ T_{CM} cells, and have been suggested to exert memory functions in peripheral tissues[34], whereas CD8⁺ T_{EM2} cells resemble differentiated CD8⁺ T_{EMRA} cells[34,37]. The role of these T cell subsets in protection against infections is still unclear. To evaluate the heterogeneity of memory CD4⁺ and CD8⁺ T cells, PBMCs collected at T0 and month 6 from 25 V_NLRs, 24 V_NHRs and 12 V_R subjects were stimulated for 24 h with peptides covering S^{WT}, S^D, S^B and S^O, or with positive (IL-2 and CD3 plus CD28 antibodies)

Fig. 5 | BNT162b2 mRNA vaccine promotes distinct memory CD4⁺ T cell profiles in V_NLR, V_NHR and V_R cohorts. a, Representative flow cytometry dot plots of CCR7 and CD27 on gated CD25⁺CD69⁺CD45RA⁻CD4⁺ T cells in V_NLRs, V_NHRs and V_R subjects at month 6, after 24h incubation with medium (unstimulated) or S^{WT}. **b–d**, Flow cytometry analysis showing the percentage of CCR7⁺CD27⁺ CD45RA⁻ T_{CM1} (**b**), CCR7⁻CD27⁺CD45RA⁻ T_{EM1} (**c**) and CCR7⁻CD27⁻CD45RA⁻ T_{EM2} (**d**) cells on gated CD25⁺CD69⁺CD4⁺ T cells collected at T0 and 6M, after 24h incubation with S^{WT}, S^D, S^O or S^B. Below: percentages of subjects with T_{CM1} (**b**), T_{EM1} (**c**) and T_{EM2} (**d**) CD25⁺CD69⁺CDR45RA⁻ CD4⁺ T cell active responses >LOS. Data are represented with background subtraction from paired unstimulated controls. The dotted black lines represent the LOD and the dotted green lines the LOS. The same subjects were longitudinally analyzed: V_NLRs (n = 25), V_NHRs (n = 24) and V_R subjects (n = 12). The box plots indicate median, IQR and minimum/maximum. Each dot of box plots represents the average across three technical replicates of the same subject; the data are pooled from multiple experiments. Statistics were calculated using two-sided Wilcoxon's signed-rank and two-sided Wilcoxon's rank-sum test. $^*P < 0.05$; $^{**}P < 0.01$.

and negative (medium) controls. The expression of several differentiation markers was assessed on gated S-specific CD25⁺CD69⁺CD4⁺ T cells and CD25⁺CD69⁺CD8⁺ T cells by flow cytometry to distinguish naive CD45RA⁺CCR7⁺CD27⁺ T cells (T_N cells), CCR7⁺CD27⁺CD45RA⁻ T_{CM1} cells, CCR7⁺CD27⁻CD45RA⁻ T_{CM2} cells, CCR7⁻CD27⁺CD45RA⁻ T_{EM1} cells, CCR7⁻CD27⁻CD45RA⁻ T_{EM2} cells and CCR7⁻CD45RA⁺T_{EMRA} cells (Fig. 5a, Extended Data Figs. 4b,c, 7a–f and 8a–f). V_R subjects had the highest frequencies of CD4⁺ T_{CM1} cells and CD4⁺ T_{EM1} cells in response to all S megapools at T0 (Fig. 5a–c and Extended Data Fig. 7a,b). Some V_N subjects (<20% of responders in all conditions) showed cross-reactive responses to S peptides of CD4⁺ T_{CM1} cells at T0 (Fig. 5b), probably as a result of T cell responses elicited after SARS-CoV-2 exposure without infection or infections with α- and β-coronaviruses[29,38–40]. The percentages of CD25⁺CD69⁺CD4⁺ T_{CM1} cells specific for S^D, S^O and S^B were significantly higher in V_NLRs at month 6 compared with T0, as well as in V_NHRs activated with all S-peptide megapools, except for S^B (Extended Data Fig. 7a). However, the frequency of S^{WT}- and S^D-specific CD4⁺ T_{CM1} cells was significantly reduced in V_NLRs compared with the frequency of S-specific CD4⁺ T_{CM1} cells in V_NHRs and V_R subjects (Fig. 5b). The frequencies of S^{WT}-specific CD4⁺ T_{EM1} cells were increased in all cohorts at month 6 compared with T0 (Extended Data Fig. 7b), but increased frequencies of polyreactive CD4⁺ T_{EM1} cells were measured only in V_NHRs (Extended Data Fig. 7b) at month 6 postvaccination. Stronger cross-reactive CD4⁺ T_{EM1} cells were also measured in V_R subjects compared with V_NHRs and V_NLRs at month 6 postvaccination (Fig. 5c). Last, the percentage of S^{WT}- and S^D-specific CD4⁺ T_{EM2} cells was significantly increased in V_NLRs after vaccination (Extended Data Fig. 7c), and they significantly increased in V_NHRs and V_NLRs compared with V_R subjects (Fig. 5d). No differences were observed when the PBMCs were stimulated with a positive control (Extended Data Fig. 8a,c,e). Higher frequencies of S-specific CD4⁺ T_N cells were measured in V_NHRs compared with V_NLRs before vaccination (T0; Extended Data Fig. 9a), suggesting a wider T cell receptor (TCR) repertoire in the T_N cell subset in V_NHRs. We did not detect differences in the percentage of CD4⁺ T_{CM2} and CD4⁺ T_{EMRA} subsets in all cohorts and timepoints (Extended Data Fig. 9b,c).

Vaccination promoted a significant increase in the magnitude of percentages of S-specific CD8⁺ T_{CM1} cells in V_NHRs (Extended Data Fig. 7d), but only S^{WT}- and S^B-specific CD8⁺ T_{CM1} cells in V_NLRs (Extended Data Fig. 7d) at month 6 postvaccination compared with T0. V_R subjects also had S-specific CD8⁺ T_{CM1} cell responses at month 6 (Fig. 6a,b and Extended Data Fig. 7d). Of note, there was a significant reduction in the response of V_NLR CD8⁺ T_{CM1} cells to S^{WT}, S^O and S^D peptide megapools compared with V_NHRs (Fig. 6b). We did not observe major differences in the reactivity of CD8⁺ T_{EM1} cells of V_NHRs compared with V_NLRs before and after vaccination (Fig. 6a,c and Extended Data Fig. 7e), whereas a significant enrichment of S-polyreactive CD8⁺ T_{EM2} cells was measured in V_NLRs at month 6 postvaccination compared with T0 (Extended Data Fig. 7f). Similar frequencies of CD8⁺ T_N cells were found at T0 and month 6 (Extended Data Fig. 9d), whereas CD8⁺ T_{CM2}- and CD8⁺ T_{EMRA}-specific responses, in terms of percentages, were barely detectable at both timepoints (Extended Data Fig. 9e,f). These observations indicated that, at month 6 postvaccination, higher frequencies of polyreactive CD4⁺ T_{CM1} cells (Fig. 5b) and CD8⁺ T_{CM1} cells (Fig. 6b) were present in V_NHRs compared with V_NLRs, whereas V_NLR memory responses were characterized by the accumulation of CD4⁺ (Fig. 5d and Extended Data Fig. 7c) and CD8⁺ (Fig. 6d and Extended Data Fig. 7f) T_{EM2} cells.

RBD antibodies and T cells correlate with COVID-19 protection. To investigate how VOC-specific immune responses are modulated after the third vaccine dose and how they correlate with protection, we examined the VOC–RBD-binding antibodies and the T cell responses against S^{WT}, S^D, S^O and S^B at 1 month post-BNT162b2 mRNA vaccine booster, which was administered to all participants at month 9 after the first dose. The RBD^{WT}- and RBD^D -binding antibody titers were reduced in V_NLRs compared with V_NHRs and V_R subjects even at month 10 (corresponding to 1 month after the third booster) (Fig. 7a, upper panel). However, the postbooster at month 10 RBD-specific antibody titers were significantly increased in all cohorts, 10-fold for RBD^{WT} and RBD^D and 100-fold for RBD^O compared with month 6 (Fig. 7a, lower panel). The fold-change for RBD^O was significantly lower in V_NLRs and V_R subjects than in V_NHRs (Fig. 7a, upper panel). At month 1 postbooster, activated CD25⁺CD69⁺CD4⁺ T cells were detected in both V_NHRs and V_NLRs after stimulation with S (Fig. 7b); however, there was no significant increase in the frequencies of S-specific CD25⁺CD69⁺CD4⁺ T cells postboost compared with month 6 postvaccination, except for the S^{WT}-specific CD25⁺CD69⁺CD4⁺ T cells in V_NHRs (Fig. 7c and Extended Data Fig. 10a). The frequencies of CD25⁺CD69⁺CD8⁺

Fig. 6 | BNT162b2 mRNA vaccine promotes distinct memory CD8⁺ T cell profiles in V_NLR, V_NHR and V_R cohorts. a, Representative flow cytometry dot plots of CCR7 and CD27 on gated CD25⁺CD45RA⁻CD69⁺ CD8⁺ T cells in V_NLRs, V_NHRs and V_R subjects at month 6, measured by flow cytometry, after 24h incubation with medium (unstimulated) or S^{WT}. **b–d**, Flow cytometry analysis showing the percentage of CCR7⁺CD27⁺CD45RA⁻ T_{CM1} (**b**), CCR7⁻CD27⁺CD45RA⁻ T_{EM1} (**c**) and CCR7⁻CD27⁻CD45RA⁻ T_{EM2} (**d**) cells among CD25⁺CD69⁺CD8⁺ T cells collected at T0 and 6M, after 24h incubation with S^{WT} or S^D, S^O and S^B. Below: percentage of subjects with T_{CM1} (**b**), T_{EM1} (**c**) and T_{EM2} (**d**) CD25⁺CD69⁺CD45RA⁻CD8⁺ T cell active responses >LOS. Data are represented with background subtraction from paired unstimulated controls. The dotted black lines represent the LOD and the dotted green lines the LOS. The same subjects were longitudinally analyzed: V_NLRs (n = 25), V_NHRs (n = 24) and V_R subjects (n = 12). The box plots indicate median, IQR and minimum/maximum. Each dot of box plots represents the average across three technical replicates of the same subject; the data are pooled from multiple experiments. Statistics were calculated using two-sided Wilcoxon's signed-rank test and two-sided Wilcoxon's rank-sum test. $^*P < 0.05$; $^{**}P < 0.01$; $^{****}P < 0.0001$.

T cells in V_NLRs were low at month 1 postboost (Fig. 7d and Extended Data Fig. 10b), without any significant increase compared with month 6 postvaccination (Fig. 7e).

Last, to test whether the different humoral responses and T_M cells' fate diversification correlated with protection, we assessed how many vaccinated individuals had breakthrough infections with

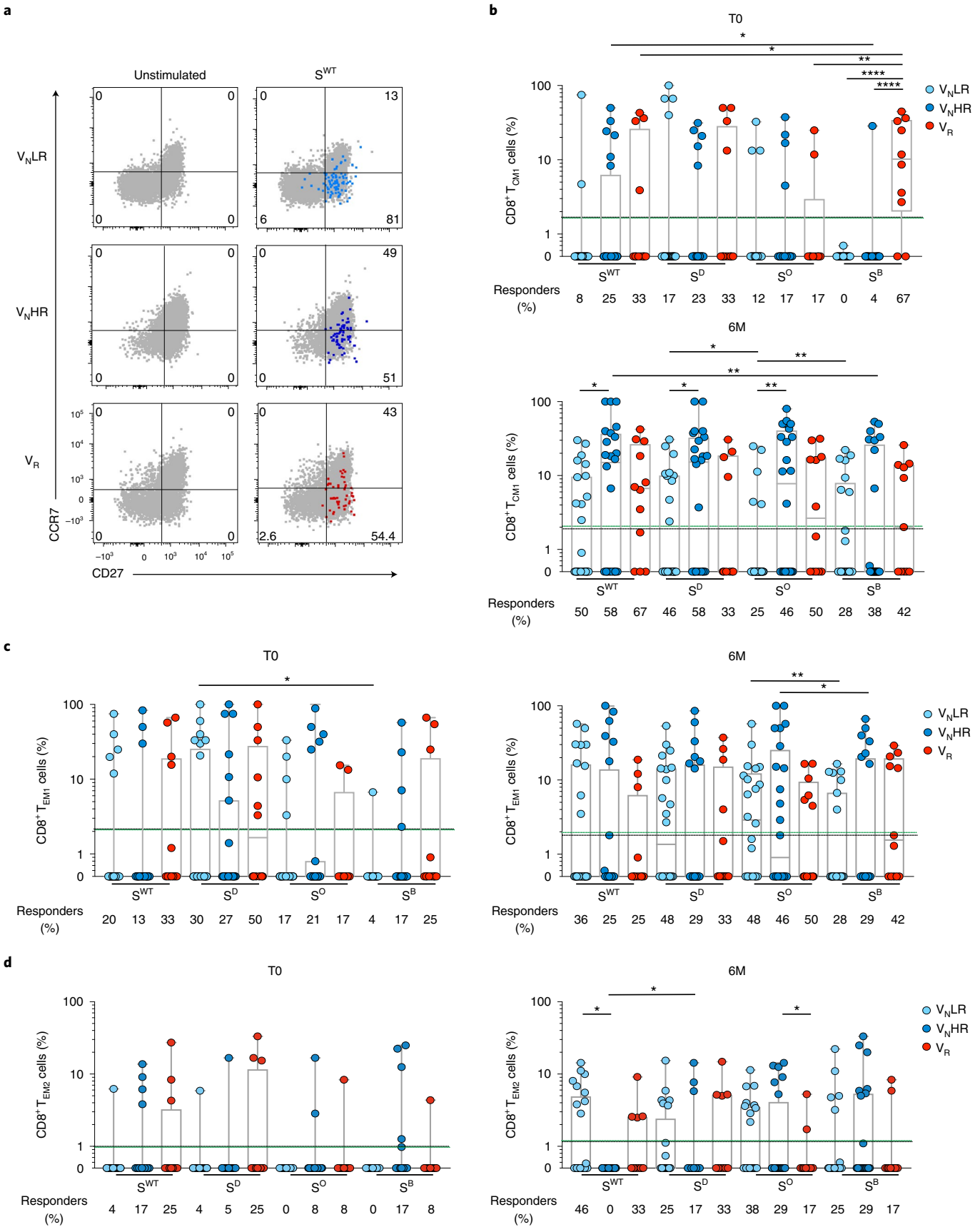

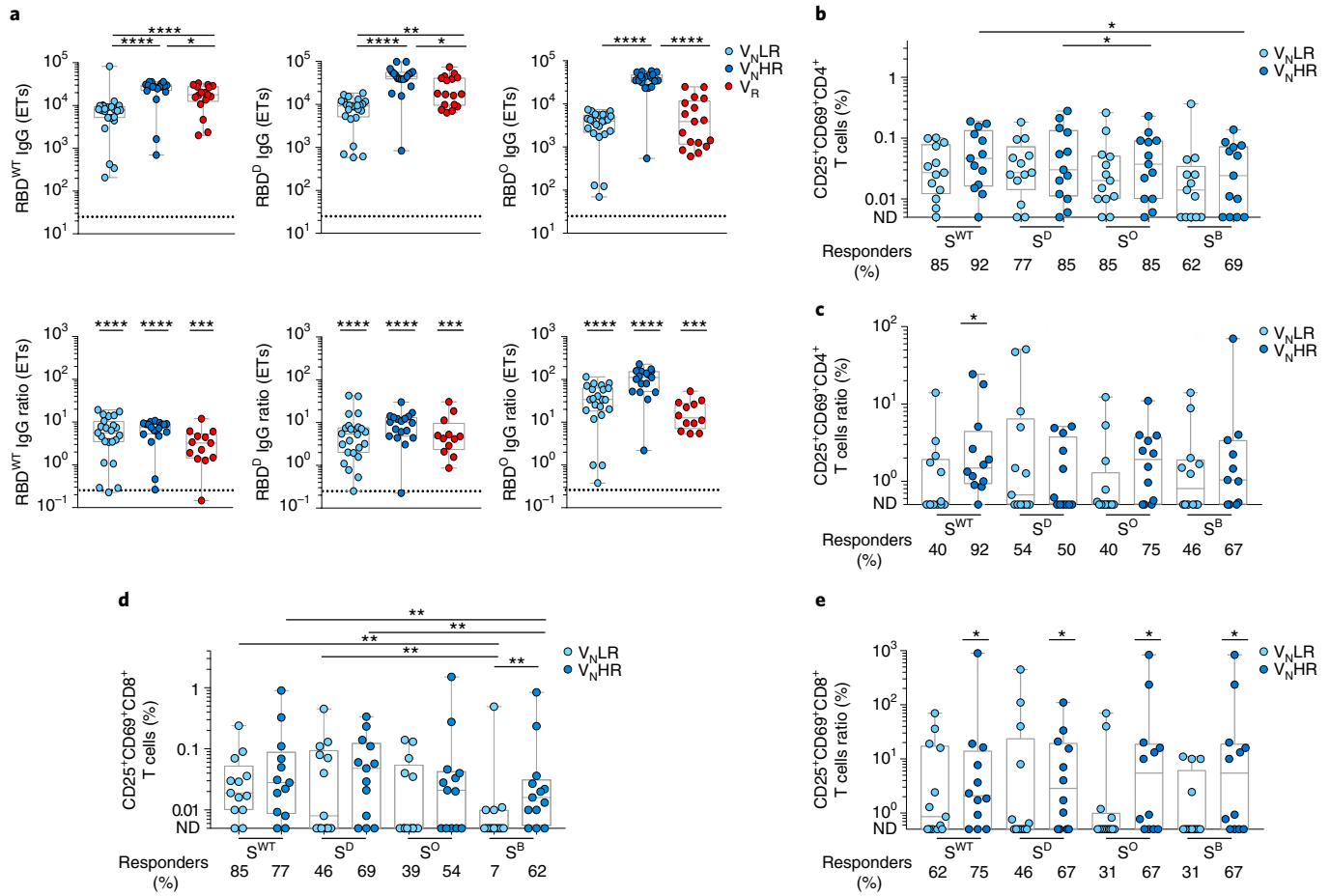

Fig. 7 | Analysis of circulating antibodies and specific CD4⁺ T cell and CD8⁺ T cell responses in V_NLRs, V_NHRs and V_R subjects after the third dose of the BNT162b2 mRNA vaccine. a, ELISA showing S-RBD^{WT}, -RBD^{D} and -RBD^{O} binding IgG titers in V_NLRs, V_NHRs and V_R subjects at month 10 (upper panel) and the corresponding ratio vs pre-boost values at month 6 (lower panel). ELISA results shown as ETs based on a standard. The dotted lines represent the LOD. At month 10: V_NLRs ($n = 24$), V_NHRs ($n = 20$) and V_R subjects ($n = 17$). At month 10 vs 6: V_NLRs ($n = 23$), V_NHRs ($n = 19$) and V_R subjects ($n = 13$). **b**–**e**, Flow cytometry analysis showing the percentage of CD25⁺CD69⁺ cells on gated CD4⁺ (**b**) and CD8⁺ (**d**) T cells from V_NLRs ($n = 13$) and V_NHRs ($n = 13$) at month 10, after 24h incubation with S^{WT}, S^{D}, S^{O} or S^{B}, and the corresponding ratio vs pre-boost values at month 6 (**c** and **e**). ND, not detected. Below: percentages of subjects with active responses >0.01. Data are represented with background subtraction from paired unstimulated controls. The same subjects were longitudinally analyzed. The box plots indicate the median, IQR and minimum/maximum. Each dot of the box plots represents the average across two (**a**) and three (**b**–**e**) technical replicates of the same subject. Statistics were calculated using two-sided Wilcoxon's signed-rank test and two-sided Wilcoxon's rank-sum test. The significance of the ratio was assessed by Wilcoxon's signed-rank *t*-test compared with a hypothetical median of 1. $^{*}P < 0.05$; $^{**}P < 0.01$; $^{***}P < 0.001$; $^{****}P < 0.0001$.

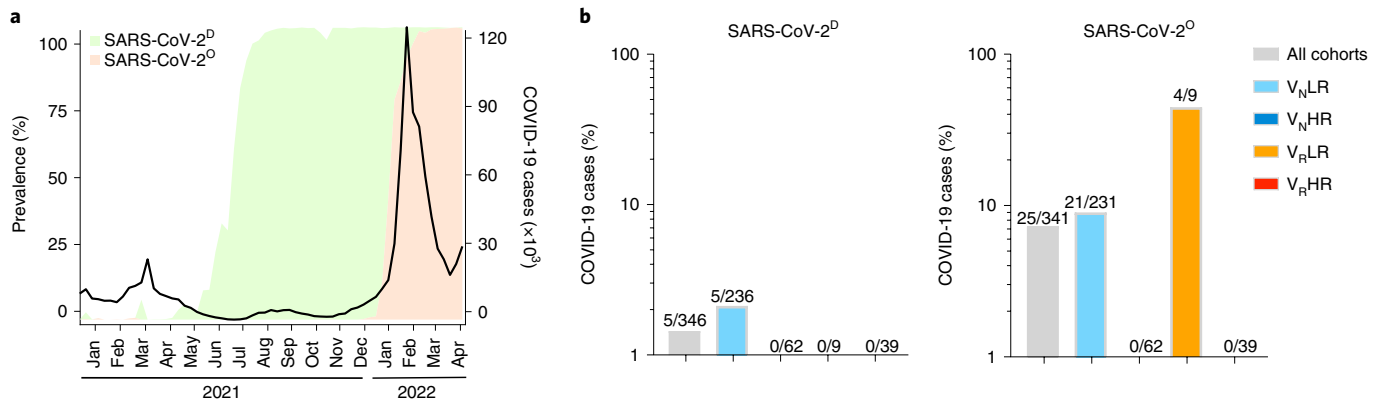

Fig. 8 | Delta and omicron breakthrough infection in V_NLRs, V_NHRs and V_R subjects. a, Prevalence of the indicated variants from January 2021 to 15 April 2022 in Italy. **b**, Percentage of COVID-19 cases correlated with the indicated SARS-CoV-2 variant breakthrough in V_NLRs, V_NHRs, V_RLRs and V_RHRs after two (left) and three (right) vaccine doses. Fisher's exact test was calculated in J ($P = 0.01$ V_NLRs versus V_NHRs; $P = 0.0006$ V_RLRs versus V_RHRs).

symptoms after immunization with two or three vaccine doses. The SARS-CoV-2 pandemic in Italy has been characterized by four distinct infection waves (www.ecdc.europa.eu), with delta accounting for >90% of the virus sequences in December 2021, and omicron for >90% since the beginning of 2022 (Fig. 8a). Of the study subjects, 1.5% (5/346) were infected with SARS-CoV-2 and developed mild COVID-19 (assessed by positive SARS-CoV-2 PCR swabs, cough and a few days of fever) within 8 months postvaccination, corresponding to the delta wave (Fig. 8b), and 7.33% (25/341) were infected with SARS-CoV-2 between 10 and 15 months postvaccination, corresponding to omicron (Fig. 8a). All subjects who developed COVID-19 symptoms after the second vaccine dose were V_NLRs (5 subjects, 2.12%), (Fig. 8b). Among the V_NLR subjects, 9.1% (21/231) developed symptomatic disease after three vaccine doses, corresponding to the omicron wave (Fig. 8b), suggesting that the reduced humoral and cellular protection in the V_NLR cohort correlated with reduced protection (Fisher's exact test, $P=0.01$). Two V_NHRs developed asymptomatic breakthrough infections during the omicron wave (Supplementary Table 2). Among the V_R subjects, 4 of the 9 V_RLRs (44.4%) developed COVID-19 (Fisher's exact test, $P=0.0006$) (Supplementary Table 2) and none of the V_RHRs (Fig. 8b). These results indicated that the reduced VOC–RBD-binding antibody titers, combined with the reduced S-specific T cell responses, correlated with the increased susceptibility of V_NLRs to break through COVID-19 caused by omicron (Supplementary Table 3).

Discussion

In the present study we show that BNT162b2 mRNA vaccine elicits broadly long-term polyreactive humoral and cellular immunity against S derived from the most widespread VOCs, including omicron. Based on the bimodal distribution of the S^{WT} IgG antibody titers at month 3 postvaccination, we subdivided the V_N subjects into V_NHRs, who showed long-lasting and higher titers of S- and RBD-specific IgGs, similar to those observed in V_R subjects, which are characterized by robust antiviral antibody responses[16–18], and V_NLRs who showed reduced titers of RBD^O-neutralizing antibodies and decreased frequencies of S^O-specific $CD8^+$ T cells. Furthermore, V_NLRs failed to control delta and omicron infection and COVID-19.

Both the nature and the dose of antigen contribute to the phenotype and the level of heterogeneity of memory and effector T cell subsets[25]. When we longitudinally analyzed the diversification and turnover rate of S-specific T_M cells generated after vaccination, we found predominantly $CD4^+$ and $CD8^+$ T_{CM1} cell responses to S^{WT}, S^B, S^D and S^O peptides in V_NHRs or V_R subjects, whereas T_{EM2} cell responses were prevalent in V_NLRs after vaccination. High frequencies of circulating $CD8^+$ T_{EM1} cells were also reported among multimer-epitope-specific $CD8^+$ T cells in blood up to 120 d after SARS-CoV-2 mRNA vaccination[30,41]. Our findings suggest that V_NHRs could have a wider crossreactive memory T cell repertoire, which can recirculate in tissues and be potentially more responsive after antigen re-encounter. Although T cell responses induced by vaccination or infection can crossrecognize S protein, as also reported by others[42–44], the frequency of IFN-γ-producing $CD4^+$ T cells and $CD8^+$ T cells were significantly lower in V_NLRs compared with the response to S^{WT}. Decreased responses against S^O have been also reported in subjects convalescent from SARS-CoV-2[44].

We used multiparametric flow cytometry to evaluate the phenotype of antigen-specific T cells following S-derived peptide stimulation in vitro. In line with previous studies[30,45], the possibility of using overlapping peptide pools, targeting multiple regions in the S protein, offers the unique opportunity to evaluate the overall T cell responses against several epitopes, thus overcoming the limitation of peptide recognition by often unknown polymorphic human leukocyte antigen (HLA) molecules. In fact, peptide–multimer labeling is often restricted to donors expressing the HLA-A2 molecule. However, our approach implies a potential caveat resulting from the possibility that peptide activation could modulate the expression of some differentiation markers expressed by S-specific T cells. The analysis of the immune phenotype of S-specific T cells at steady state will require further deeper investigations and the development of new methodological approaches.

Some similarities between V_NHRs and V_R subjects support the hypothesis of previous viral exposure[46] in V_NHRs. In these subjects, vaccination may provide a long-term, polyspecific, immunological memory. Consistent with this hypothesis, robust polyreactive memory $CD8^+$ T cells were reported in a large cohort of hepatitis C virus (HCV)-exposed individuals who did not develop hepatitis and were negative for HCV RNA and anti-HCV antibody[46]. Pre-existing RNA polymerase-specific T cells have been reported in SARS-CoV-2-exposed individuals, without any evidence of infection[47].

Both humoral and cellular immunity protect from SARS-CoV-2 challenge in macaques. $CD8^+$ T cell depletion in infected macaques causes breakthrough virus infection, documented by nasal swabs, after re-challenge with SARS-CoV-2[48]. In this model, viral control postvaccination with adenoviral vectors correlates with both antibody and T cell responses, and with protection against the highly mutated omicron variant[12]. These findings suggest that $CD8^+$ T cells can continue to be protective at timepoints when neutralizing antibody titers decline or are below the threshold of host protection[48]. Accordingly, the decreased anti-RBD-binding antibody titers associated with reduced S-specific T cell responses in V_NLR subjects could account for the reduced protection observed in this group.

We observed a higher percentage of females among V_NHRs compared with V_NLRs. Little is known about how sex may impact the immunogenicity and protection elicited by mRNA vaccine. Age- and frailty-associated decrease in humoral responses is greater in males than in females[49]. The age-related decreases in antibody titers observed in males have been also associated with a decline in $CD4^+$ T cell responses[50].

In the present study, we describe three main categories of responders to mRNA vaccination on the basis of S- and RBD-specific IgG titers, S-reactive B cells and polyreactive T_M cells. Our results suggest that protection against highly mutated VOCs relied on the contribution of both humoral and cellular immunity. The distinct phenotype and frequency of $CD4^+$ and $CD8^+$ T_M cell subsets detected in V_NLRs correlated with reduced protection against COVID-19. Further investigations are needed to fully elucidate the mechanisms of differentiation of the various T cell subclasses, and how they evolve postvaccination, in parallel with the clinical outcome. In this context, analysis of the evolution of the TCR repertoire might help elucidate the distinct differentiation paths. Altogether, our observations will contribute to determine protocols to monitor long-term memory responses, and to design new vaccination and targeted booster protocols, especially for at-risk individuals.

Online content

Any methods, additional references, Nature Research reporting summaries, extended data, supplementary information, acknowledgements, peer review information; details of author contributions and competing interests; and statements of data and code availability are available at https://doi.org/10.1038/s41590-022-01313-z.

Received: 18 January 2022; Accepted: 10 August 2022;
Published online: 22 September 2022

References

1. Fisher, D. & Wilder-Smith, A. The global community needs to swiftly ramp up the response to contain COVID-19. *Lancet* **395**, 1109–1110 (2020).
2. Celardo, I., Pace, L., Cifaldi, L., Gaudio, C. & Barnaba, V. The immune system view of the coronavirus SARS-CoV-2. *Biol. Direct* **15**, 30 (2020).
3. Thomas, S. J. et al. Safety and efficacy of the BNT162b2 mRNA Covid-19 vaccine through 6 months. *N. Engl. J. Med.* **385**, 1761–1773 (2021).

4. Moderna. Moderna Reports Second Quarter Fiscal Year 2021 Financial Results and Provides Business Updates. Press release (2021).
5. Regev-Yochay, G. et al. Decreased infectivity following BNT162b2 vaccination: a prospective cohort study in Israel. *Lancet Reg. Health Eur.* **7**, 100150 (2021).
6. Baden, L.R. et al. Efficacy and safety of the mRNA-1273 SARS-CoV-2 vaccine. *N. Engl. J. Med.* **384**, 403–416 (2021).
7. Polack, F. P. et al. Safety and efficacy of the BNT162b2 mRNA Covid-19 vaccine. *N. Engl. J. Med.* **383**, 2603–2615 (2020).
8. Pegu, A. et al. Durability of mRNA-1273 vaccine-induced antibodies against SARS-CoV-2 variants. *Science* **373**, 1372–1377 (2021).
9. Altmann, D. M. & Boyton, R. J. SARS-CoV-2 T cell immunity: specificity, function, durability, and role in protection. *Sci. Immunol.* **5**, eabd6160 (2020).
10. Channappanavar, R., Fett, C., Zhao, J., Meyerholz, D. K. & Perlman, S. Virus-specific memory CD8 T cells provide substantial protection from lethal severe acute respiratory syndrome coronavirus infection. *J. Virol.* **88**, 11034–11044 (2014).
11. Gallais, F. et al. Intrafamilial exposure to SARS-CoV-2 associated with cellular immune response without seroconversion, France. *Emerg. Infect. Dis.* **27**, 113–121 (2021).
12. Chandrashekar, A. et al. Vaccine protection against the SARS-CoV-2 omicron variant in macaques. *Cell* **185**, 1549–1555e1511 (2022).
13. Abu-Raddad, L. J. et al. SARS-CoV-2 antibody-positivity protects against reinfection for at least seven months with 95% efficacy. *eClinicalMedicine* **35**, 100861 (2021).
14. Hall, V. J. et al. SARS-CoV-2 infection rates of antibody-positive compared with antibody-negative health-care workers in England: a large, multicentre, prospective cohort study (SIREN). *Lancet* **397**, 1459–1469 (2021).
15. Lumley, S. F. et al. Antibody status and incidence of SARS-CoV-2 infection in health care workers. *N. Engl. J. Med.* **384**, 533–540 (2021).
16. Barda, N. et al. Safety of the BNT162b2 mRNA Covid-19 vaccine in a nationwide setting. *N. Engl. J. Med.* **385**, 1078–1090 (2021).
17. Schmidt, F. et al. High genetic barrier to SARS-CoV-2 polyclonal neutralizing antibody escape. *Nature* **600**, 512–516 (2021).
18. Stamatatos, L. et al. mRNA vaccination boosts cross-variant neutralizing antibodies elicited by SARS-CoV-2 infection. *Science* **372**, 1413–1418 (2021).
19. Rodda, L. B. et al. Imprinted SARS-CoV-2-specific memory lymphocytes define hybrid immunity. *Cell* **185**, 1588–1601.e14 (2022).
20. Gaebler, C. et al. Evolution of antibody immunity to SARS-CoV-2. *Nature* **591**, 639–644 (2021).
21. Wang, Z. et al. Naturally enhanced neutralizing breadth against SARS-CoV-2 one year after infection. *Nature* **595**, 426–431 (2021).
22. Anderson, E. J. et al. Safety and Immunogenicity of SARS-CoV-2 mRNA-1273 vaccine in older adults. *N. Engl. J. Med.* **383**, 2427–2438 (2020).
23. Sahin, U. et al. COVID-19 vaccine BNT162b1 elicits human antibody and TH1 T cell responses. *Nature* **586**, 594–599 (2020).
24. Lederer, K. et al. SARS-CoV-2 mRNA vaccines foster potent antigen-specific germinal center responses associated with neutralizing antibody generation. *Immunity* **53**, 1281–1295.e1285 (2020).
25. Pace, L. Temporal and epigenetic control of plasticity and fate decision during CD8$^+$ T-cell memory differentiation. *Cold Spring Harb. Perspect. Biol.* **13**, a037754 (2021).
26. Jarjour, N. N., Masopust, D. & Jameson, S. C. T cell memory: understanding COVID-19. *Immunity* **54**, 14–18 (2021).
27. Jameson, S. C. & Masopust, D. Understanding subset diversity in T cell memory. *Immunity* **48**, 214–226 (2018).
28. Tarke, A. et al. SARS-CoV-2 vaccination induces immunological T cell memory able to cross-recognize variants from alpha to omicron. *Cell* **185**, 847–859.e811 (2022).
29. Mateus, J. et al. Low-dose mRNA-1273 COVID-19 vaccine generates durable memory enhanced by cross-reactive T cells. *Science* **374**, eabj9853 (2021).
30. Goel, R. R. et al. mRNA vaccines induce durable immune memory to SARS-CoV-2 and variants of concern. *Science* **374**, eabm0829 (2021).
31. Cao, Y. et al. Omicron escapes the majority of existing SARS-CoV-2 neutralizing antibodies. *Nature* **602**, 657–663 (2022).
32. Cele, S. et al. Omicron extensively but incompletely escapes Pfizer BNT162b2 neutralization. *Nature* **602**, 654–656 (2022).
33. Grifoni, A. et al. SARS-CoV-2 human T cell epitopes: aaptive immune response against COVID-19. *Cell Host Microbe* **29**, 1076–1092 (2021).
34. Romero, P. et al. Four functionally distinct populations of human effector-memory CD8+ T lymphocytes. *J. Immunol.* **178**, 4112–4119 (2007).
35. Sallusto, F., Lenig, D., Forster, R., Lipp, M. & Lanzavecchia, A. Two subsets of memory T lymphocytes with distinct homing potentials and effector functions. *Nature* **401**, 708–712 (1999).
36. Mathew, D. et al. Deep immune profiling of COVID-19 patients reveals distinct immunotypes with therapeutic implications. *Science* **369**, eabc8511 (2020).
37. Giles, J. R. et al. Human epigenetic and transcriptional T cell differentiation atlas for identifying functional T cell-specific enhancers. *Immunity* **55**, 557–574.e557 (2022).
38. Braun, J. et al. SARS-CoV-2-reactive T cells in healthy donors and patients with COVID-19. *Nature* **587**, 270–274 (2020).
39. Grifoni, A. et al. Targets of T cell responses to SARS-CoV-2 coronavirus in humans with COVID-19 disease and unexposed individuals. *Cell* **181**, 1489–1501.e1415 (2020).
40. Sekine, T. et al. Robust T cell immunity in convalescent Individuals with asymptomatic or mild COVID-19. *Cell* **183**, 158–168.e114 (2020).
41. Oberhardt, V. et al. Rapid and stable mobilization of CD8$^+$ T cells by SARS-CoV-2 mRNA vaccine. *Nature* **597**, 268–273 (2021).
42. Lan, J. et al. Structure of the SARS-CoV-2 spike receptor-binding domain bound to the ACE2 receptor. *Nature* **581**, 215–220 (2020).
43. GeurtsvanKessel, C. H. et al. Divergent SARS-CoV-2 omicron-reactive T and B cell responses in COVID-19 vaccine recipients. *Sci. Immunol.* **7**, eabo2202 (2022).
44. Keeton, R. et al. T cell responses to SARS-CoV-2 spike cross-recognize omicron. *Nature* **603**, 488–492 (2022).
45. Mateus, J. et al. Selective and cross-reactive SARS-CoV-2 T cell epitopes in unexposed humans. *Science* **370**, 89–94 (2020).
46. Scognamiglio, P. et al. Presence of effector CD8+ T cells in hepatitis C virus-exposed healthy seronegative donors. *J. Immunol.* **162**, 6681–6689 (1999).
47. Swadling, L. et al. Pre-existing polymerase-specific T cells expand in abortive seronegative SARS-CoV-2. *Nature* **601**, 110–117 (2021).
48. McMahan, K. et al. Correlates of protection against SARS-CoV-2 in rhesus macaques. *Nature* **590**, 630–634 (2021).
49. Shapiro, J. R. et al. Association of frailty, age, and biological sex with SARS-CoV-2 mRNA vaccine-induced immunity in older adults. *Clin. Infect. Dis.* **75**(Suppl. 1), S61–S71 (2022).
50. Bai, J. et al. Sex, age, and ethnic background shape adaptive immune responses induced by the SARS-CoV-2 mRNA vaccine. *Front. Immunol.* **13**, 786586 (2022).

Methods

Cohort. In total, 379 staff members of CCI were recruited for the study (Supplementary Table 1). CCI is a certified COVID-free oncological hospital. All the employers have been constantly tested for SARS-CoV-2 infection by PCR following a stringent schedule. Starting from February 2020 to date, each individual has been screened: every 2–4 weeks (subjects were chosen randomly during this timeframe to ensure a daily check in each branch of the hospital); after 5 days out of office; and after close contact with a SARS-CoV-2-infected subject. In case of close contact with an infected subject, participants were isolated in quarantine for 14 days; during this timeframe, they were PCR tested each week until December 2021 or PCR screened every day for 2 weeks (from January 2022). All participants were tested for N^{WT} and S^{WT} IgG levels in plasma at T0.

Participants classified as V_N were classified into V_NLRs, V_NHRs and nonresponders (NRs). NRs were characterized by S^{WT} IgG values <50 a.u. ml^{-1} at 6 weeks after vaccination and the remaining naive subjects' IgG values were used to define a threshold to discriminate between V_NLRs and V_NHRs, leveraging 3 months of IgG data. The distribution of 3-month IgG values for multimodality was tested ($P < 2.2 \times 10^{-16}$, excess mass test) and the antimode (135 a.u. ml^{-1}) was located with the expectation of a bimodal data distribution. This antimode value was used to discriminate between V_NLRs and V_NHRs (<135 a.u. ml^{-1} and >135 a.u. ml^{-1} at 3 months, respectively). In addition, subjects with IgG titers >5 a.u. ml^{-1} at T0 were defined as seropositive.

Subjects with a documented SARS-CoV-2 infection who recovered from COVID-19 with mild symptoms (subjects with post-acute COVID-19 syndrome, long COVID or lingering symptoms were not included in the study) were classified into V_RLRs and V_RHRs with the same methodology applied for naive subjects: 3-month IgG values were tested for multimodality ($P = 0.49$, excess mass test) and split using the antimode 112 a.u. ml^{-1} located with the expectation of a bimodal data distribution. For the analysis shown in Figs. 2–7, subjects in each class were ranked according to three criteria: (1) subjects were split into three age categories (reported in order of priority for analysis): from 40 years old (y.o.) to 50 y.o., <40 y.o. and >50 y.o.; (2) in these age categories, subjects were ranked by age (from youngest to oldest); and (3) in these age categories, subjects were ranked by measured IgG values at 3 months (from highest to lowest). In addition the gender was also taken into consideration. The top ranking subjects from each class were selected for analysis. According to the S^{WT} IgG quantification and the ranking mentioned above, we decided to focus our analysis on 123 subjects who received the BNT162b2 vaccination (Supplementary Table 2). These subjects were divided into three groups: 43 V_NLRs, 42 V_NHRs and 38 V_R donors. Blood samples were collected before the first BNT162b2 mRNA (Comirnaty, Pfizer Biontech) vaccine dose (T0), before the second vaccine dose (week 3) and after 6 weeks, 3 and 6 months from the first immunization. Blood samples were also collected 1 month after the third vaccine dose (10 months after T0). 96% of donors received BNT162b2 mRNA vaccine as third dose, whereas the remaining 4% received mRNA-1273 Moderna vaccine. Data shown in Fig. 2 to 7 and in Extended Data Fig. 2 to 9 were obtained from donors immunised with BNT162b2 mRNA vaccine. All donors signed informed consent forms approved by the Ethical Committee of the CCI; participants did not receive compensation.

Sample processing. Blood samples were collected into heparin tubes via phlebotomy. Tubes were centrifuged at 800*g* for 5 min and 4 °C to separate plasma that was used for serological analysis. Whole blood was diluted 1:1 with phosphate-buffered saline (PBS) 1× (Sigma-Aldrich) and PBMC isolation was obtained by density gradient centrifugation using Lympholyte (Cederlane). Tubes were centrifuged at 805*g* for 30 min at room temperature and PBMCs were collected into new tubes. Cells were washed with PBS 1×, centrifuged at 515*g* for 10 min and 4 °C, counted with the Burker chamber and cryopreserved in 10% dimethyl sulfoxide in fetal bovine serum (FBS; BioWest).

Spike IgM and IgG quantification. Chemiluminescence immunoassay was performed with TGS COVID-19 Control Set (Technogenetics CVCLCSGM), TGS COVID-19 IgM (CVCL100M) and TGS COVID-19 IgG (CVCL100G) according to the manufacturers' instructions to quantify IgM and IgG.

Recombinant N^{WT}, S^{WT}-, S^{D}-, S^{O}- and S^{B}-RBD antigen expression and purification. Recombinant SARS-CoV-2 N- and S-RBDs were produced using poly(ethyleneimine)-based transient transfection of Freestyle HEK293 Cells (HEK293-F, Life Technologies) cultivated in suspension. Briefly, cell medium containing the secreted proteins of interest was collected 6 d after transfection by centrifugation at 1,000*g* for 15 min. The samples were loaded on to a 5-ml His-Trap excel column (Cytiva) using a peristaltic pump and then eluted with 3–250 mM imidazole gradient using an NGC fast protein liquid chromatography system (BioRad). Peak fractions containing the antigens of interest were subjected to immediate concentration with concomitant buffer exchange with fresh PBS to remove imidazole using Amicon centrifugal filters (Merck). Quality controls during protein purification were carried out using reducing and nonreducing sodium dodecylsulfate–polyacryamide gel electrophoresis analysis and differential scanning fluorimetry with a Tycho NT.6 instrument (Nanotemper). All samples were concentrated to 1 mg ml^{-1}, flash-frozen in liquid nitrogen and kept at −80 °C until usage.

ELISA. SARS-CoV-2 N and SARS-CoV-2 S-RBD-specific-binding IgG antibodies were longitudinally tested by ELISA. Maxisorp ELISA 96-well plates (Thermo Fisher Scientific) were coated with 1 µg ml^{-1} of SARS-CoV-2 nucleocapsid or 2 µg ml^{-1} of S -RBD^{WT},-RBD^{D} or -RBD^{O} protein in 1× DPBS and incubated at 4 °C overnight. After incubation, plates were washed 3× with PBS containing 0.1% Tween-20 (PBS-T) and blocked with PBS-T supplemented with 3% bovine serum albumin (BSA; Sigma-Aldrich) for 1 h at room temperature. After washing, plasma was added and incubated for 1.5 h at room temperature. Plasma was diluted in 1% BSA in PBS-T starting from 1:25 or 1:100 dilution and serially diluting each sample by 1:4. Plates were washed 3× with PBS-T and then the secondary antibody (anti-human IgG peroxidase, BD), in 1% BSA and PBS-T, was added and the plates were incubated for 1 h at room temperature. After three washes with PBS-T, plates were developed with TMB Substrate Kit (Thermo Fisher Scientific) at room temperature. The reaction was stopped with 1 M chloridric acid and the plates were read on a Tecan Spark plate reader at 450 nm. Optical densities (ODs) were background subtracted. A positive control standard was created by pooling plasma from six V_R subjects, whereas a negative control standard was created by pooling plasma from six pre-pandemic processed plasma samples. Positive and negative control standards were run on each plate. The limit of detection (LOD) was defined as 1:25 for IgG or otherwise stated. The limit of sensitivity (LOS) was established on the basis of uninfected subjects, using plasma from donors never exposed to SARS-CoV-2. For each sample, the ELISA endpoint titer was calculated using nonlinear regression interpolation curve fitting based on the positive control standard. Titers were calculated as the reciprocal serum dilution that yields a corrected OD value of 0.1. Similar results were achieved using Sino Biological SARS-CoV-2 S-RBD proteins.

HEK293TN-hACE2 cell-line generation. HEK293TN-hACE2 (human angiotensin-converting enzyme 2) cell line was generated by lentiviral transduction of HEK293TN cells. HEK293TN cells were obtained from System Bioscience. Lentiviral vectors were produced following a standard procedure based on calcium phosphate co-transfection with third-generation helper and transfer plasmids. The following helper vectors were used (gifts from D. Trono): pMD2.G/VSV-G (Addgene, catalog no. 12259), pRSV-Rev (Addgene, catalog no. 12253) and pMDLg/pRRE (Addgene, catalog no. 12251). The transfer vector pLENTI_hACE2_HygR was obtained by cloning of hACE2 from pcDNA3.1-hACE2 (a gift from F. Li, Addgene, catalog no. 145033) into pLenti-CMV-GFP-Hygro (a gift from E. Campeau and P. Kaufman, Addgene, catalog no. 17446). The hACE2 cDNA was amplified by PCR and inserted under the cytomegalovirus promoter of the pLenti-CMV-GFP-Hygro after green fluorescent protein (GFP) excision with XbaI and SalI digestion; pLENTI_hACE2_HygR is now available through Addgene (catalog no. 155296). After transduction with hACE2 lentiviral vector, cells were subjected to antibiotic selection with hygromycin at 250 µg ml^{-1}. Expression of hACE2 cells was confirmed by flow cytometry staining using anti-hACE2 primary antibody (AF933, R&D Systems) and rabbit anti-goat IgG secondary antibody (Alexa Fluor-647). HEK293TN-hACE2 cells were maintained in Dulbecco's modified Eagle's medium (DMEM), supplemented with 10% FBS, 1% glutamine, 1% penicillin–streptomycin and 250 µg ml^{-1} of hygromycin (Gibco) and expression of hACE2 was found to be stable after multiple passages.

Plasmids and molecular cloning. The pCAGGS plasmid containing the sequence encoding for carboxy-terminal, His-tagged Wuhan SARS-CoV-2 Spike RBD (catalog no. NR_52310) was obtained from BEI Resources. Variants were generated by replacing the SARS-Cov-2 Wuhan RBD-encoding sequence with synthetic sequences (Genewiz), encoding for either SARS-CoV-2 RBD delta or SARS-CoV-2 RBD omicron variants into the pCAGGS plasmid template using the 5′-XbaI and 3′-NotI restriction sites.

Production of SARS-CoV-2 pseudoparticles. To generate lentiviral particles pseudotyped with SARS-CoV-2 S, we constructed a series of expression plasmids each encoding a SARS-CoV-2 S mutant. Briefly, for each variant, the corresponding C-terminal-deleted (19 amino acids) S complementary DNA was cloned in pcDNA3.1. Then, pLenti CMV-GFP-TAV2A-LUC Hygro was generated from pLenti-CMV-GFP-Hygro (Addgene, catalog no. 17446) by addition of T2A-Luciferase through PCR cloning. To produce the pseudotyped lentiviral particles, 5×10^6 HEK293TN cells were plated in a 15-cm dish in complete DMEM medium and co-transfected on the following day with 32 µg of plasmid pLenti CMV-GFP-TAV2A-LUC Hygro, 12.5 mg of pMDLg/pRRE (Addgene, catalog no. 12251), 6.25 mg of pRSV-Rev (Addgene, catalog no. 12253) and 9 µg of S plasmid. The medium was replaced with complete Iscove's modification of DMEM 12 h before transfection. Some 30 h after transfection, the supernatant was collected, clarified by filtration through 0.45-µm pore-size membranes and concentrated by ultracentrifugation (SW32Ti rotor). Viral pseudoparticle suspensions were aliquoted and stored at −80 °C.

Neutralization assay. For the neutralization assay with pseudotyped particles, HEK293TN-hACE2 cells were plated 10,000 per well in white 96-well plates in complete DMEM. After 24 h, cells were transduced with 0.1 multiplicity of infection of SARS-CoV-2 pseudovirus previously incubated with a serial threefold dilution of inactivated plasma to obtain a 7-point dose–response curve. Then, 5 µl of each dilution was added to 45 µl of DMEM containing the pseudovirus and incubated for 1 h at 37 °C. The serum/pseudovirus mixture, 50 µl, was then added to each well and the plates were incubated for 24 h at 37 °C. Each point was assayed in triplicate. After 24 h of incubation, cell transduction was measured by luciferase assay using Bright-Glo Luciferase System (Promega) and Infinite F200 plate reader (Tecan). Measured relative light units were normalized with respect to controls and dose–response curves were generated and neutralization dose 50 (ND_{50}) calculated by nonlinear regression curve fitting with GraphPad Prism.

In vitro stimulation. Frozen PBMCs were thawed in complete medium (RPMI supplemented with 2.5% human serum from Aurogene, 1% L-glutamine, 1% penicillin–streptomycin, 1% nonessential amino acids, 1% sodium pyruvate and 0.1% 2-mercaptoethanol). PBMCs were centrifuged at 515*g* for 10 min and 4 °C, counted with the Burker chamber and resuspended in complete medium. PBMCs were cultured for either 14 h or 24 h with peptide megapools, prepared as previously described[28], consisting in overlapping 15-mers by 10 amino acids covering the complete sequence of the S protein of the WT SARS-CoV-2 (GenBank, accession no. MN_908947) as well as beta, delta and omicron SARS-CoV-2 variants (1 µg ml^{-1}). Complete medium was used as a negative control. Dynabeads human T-activator CD3/CD28 (from Gibco, 1:1 bead:cell ratio) supplemented with human (h)IL-2 (from Novartis, 40 U ml^{-1}) was included as a positive control. To analyze the effector and cytotoxic functions, after 14 h of incubation, PBMCs were stimulated with phorbol 12-myristate 13-acetate (Sigma-Aldrich, 20 ng ml^{-1}) and ionomycin (Sigma-Aldrich, 1 µg ml^{-1}). After 1 h, Brefeldin A (Sigma-Aldrich, 5 µg ml^{-1}) was added and the combined treatment lasted 4 h more. For each condition, triplicate wells containing 3×10^5 cells in 200 µl were plated in 96-well round-bottomed plates and incubated at 37 °C with 5% CO_2. The same subjects have been analyzed longitudinally.

Intra-/extracellular staining and flow cytometry analysis. After 14 h of incubation, PBMCs were stained for intracellular cytokines combined with surface markers, whereas after 24 h PBMCs were stained for only surface markers. Cells were washed with 1× PBS supplemented with 0.5% BSA and 2 mM EDTA (FACS buffer) and stained with Fixable Viability Stain 450 in 1× PBS for 20 min at 4 °C to discriminate viable from nonviable cells. Then PBMCs were labeled with the following antibodies for multiparametric flow cytometry analysis: anti-CD3 (BD, SK7, 1:200), anti-CD4 (BD, RPA-T4, 1:400), anti-CD8 (BD, SK1, 1:600), anti-CD14 (BD, MφP9, 1:200), anti-CD16 (BD, 3G8, 1:600), anti-CD19 (BD, HIB19, 1:600), anti-CD25 (BD, 2A3, 1:200), anti-CD27 (BD, M-T271, 1:50), anti-CD45RA (BD, HI100, 1:50), anti-CD45RA (BD, 5H9, 1:200), anti-CD56 (BD, NCAM16.2, 1:200), anti-CD45RO (BD, UCHL-1, 1:200), anti-CD69 (BD, FN50, 1:50), anti-CD197 (BD, 150503, 1:100), anti-IFN-γ (BD, B27, 1:50), anti-IL-2 (BD, MQ1-17H12, 1:100), anti-Granzyme B (BD, GB11, 1:100) and anti-TNF-α (BD, MAb11, 1:100). Dilutions are indicative, because each antibody batch has been titrated. Surface staining was performed in FACS buffer for 30 min at 4 °C. Then, cells were washed and fixed with 1% paraformaldehyde in 1× PBS. For the intracellular cytokines staining, after fixation, cells were permeabilized with 1× Perm/Wash buffer (BD) according to the manufacturer's instructions and stained for 1 h at room temperature in BD Perm/Wash buffer. Cells were then washed twice and resuspended in FACS buffer for data acquisition. The same subjects have been analyzed longitudinally. Flow cytometry data were acquired on a BD LSR Fortessa X-20 instrument and analyzed with FlowJo software. The LOD for antigen-specific $CD4^+$ and $CD8^+$ T cell responses was calculated as the geomean twofold s.d. from the negative control (unstimulated). The LOS for antigen-specific $CD4^+$ and $CD8^+$ T cell responses was calculated as the median twofold s.d. from the negative control (unstimulated)[28]. When LOD and LOS were negative or 0, we considered as active responses only those >0.01 after background subtraction. No detected responses are labeled ND.

Detection of SARS-CoV-2 antigen-specific B cells. The analysis of SARS-CoV-2 antigen-specific B cells was performed using the SARS-CoV-2 B Cell Analysis Kit (Miltenyi) according to the manufacturer's instructions. PBMCs were labeled with two tetramers formed from a recombinant SARS-CoV-2 S^{WT} protein (conjugated with phycoerythrin (PE) and PE-Vio), combined with the following antibodies: anti-CD19, anti-CD27, anti-IgG, anti-IgA and anti-IgM.

Analysis of VOC prevalence. Aggregated GISAID (https://doi.org/10.1002/gch2.1018) and aggregated COVID-19 case data for the percentage distribution of VOCs in Italy was downloaded from the European Centre for Disease Prevention and Control (https://www.ecdc.europa.eu/en/publications-data/data-virus-variants-covid-19-eueea; access date 15 April 2022).

Statistical analysis. Wilcoxon's signed-rank (nonparametric, paired), Wilcoxon's rank-sum (nonparametric, unpaired) and Spearman's correlation tests were used for statistical analysis and the *P* value was determined using Prism software (Graphpad Software, Inc.), or otherwise as indicated in the text. Significance of ratio was assessed by Wilcoxon's signed-rank *t*-test compared with a hypothetical median of 1. $^*P<0.05$, $^{**}P<0.01$, $^{***}P<0.001$, $^{****}P<0.0001$.

Reporting summary. Further information on research design is available in the Nature Research Reporting Summary linked to this article.

Acknowledgements

We thank M. Olivero, L. Palmas, R. Albano and D. Baev for helpful discussion and technical support, the CCI and AVIS volunteers for donating their blood and the nurses for their assistance. We thank all the IIGM and CCI colleagues for helpful discussions and all technicians for help. We thank A. Pinnola for support with molecular cloning and A. Canciani for support with antigen purification. L.P. received founding from IIGM/CSP, Armenise-Harvard Foundation, Ministero della Salute 'COVID-2020–12371849', FPO/Candiolo Advance 5×1000_2018 'Im-MEMORY'; A. Sapino received funding from FPRC 5×1,000 M.I.U.R 2017 'INTERONC-EMALAB', FPO 5×1000 Ministero Salute 2018 'EMALAB', Ministero Salute Ricerca Corrente 2021. F.F. received funding from Armenise-Harvard Foundation, AIRC 'MFAG 20075', NATO 'SPS G5701', Velux Stiftung '1375', Mizutani Foundation for Glycoscience '200039' and MUR (Dipartimenti di Eccellenza 2018–2022); and obtained funding through BEI Resources, the National Institute of Allergy and Infectious Diseases (NIAID), National Institutes of Health (NIH): vector pCAGGS containing the SARS-related coronavirus 2, Wuhan-Hu-1 spike glycoprotein receptor-binding domain (RBD) (no. NR-52309). A.Sette received founding from federal funds from the NIAID, NIH and Department of Health and Human Services under contract no. 75N93021C00016, and V.B. from AIRC (no. IG-2017 ID 19939).

Author contributions

L.P., A. Sottile, A. Sapino and V.B. conceived the project. L.P., A. Sottile, A. Sapino, V.B., I.E., N.B., G.M., S.A.S., V.R., C.DI., K.G., D.B., F.F. A.G., A.S., S.M., R.D., S.M. and F.F. performed the methodology. I.E., N.B., G.M., S.A.S., V.R., C.DI., K.G., D.B., F.F., M. Macagno, M. Montone and B.M. carried out the investigations. L.P., A. Sottile, A. Sapino, V.B., I.E., N.B., G.M., S.A.S., V.R. and C.D.I. visualized the study. L.P., A. Sottile, A. Sapino and V.B. acquired the funding. L.P., A. Sottile and A. Sapino administered the project. L.P., A. Sottile and A. Sapino supervised the project. L.P., V.B., A. Sapino, I.E., S.A.S., V.R. and C.D.I. wrote the manuscript.

Competing interests

A.Sette is a consultant for Gritstone Bio, Flow Pharma, Arcturus Therapeutics, ImmunoScape, CellCarta, Avalia, Moderna, Fortress and Repertoire. All other authors declare no conflicts of interest. L.J.I. has filed for patent protection for various aspects of T cell epitope and vaccine design work. CCI. has filed a patent for immune correlate of protection after RNA vaccination. R.D.F. is a consultant for Moderna Inc. The data are tabulated in the main paper and in the supplementary materials.

Additional information

Extended data Extended data are available for this paper at https://doi.org/10.1038/s41590-022-01313-z.

Supplementary information The online version contains supplementary material available at https://doi.org/10.1038/s41590-022-01313-z.

Correspondence and requests for materials should be addressed to Luigia Pace.

Peer review information *Nature Immunology* thanks Tao Dong, Mala Maini and the other, anonymous, reviewer(s) for their contribution to the peer review of this work. Primary Handling Editor:Ioana Visan, in collaboration with the *Nature Immunology* team.

Reprints and permissions information is available at www.nature.com/reprints.

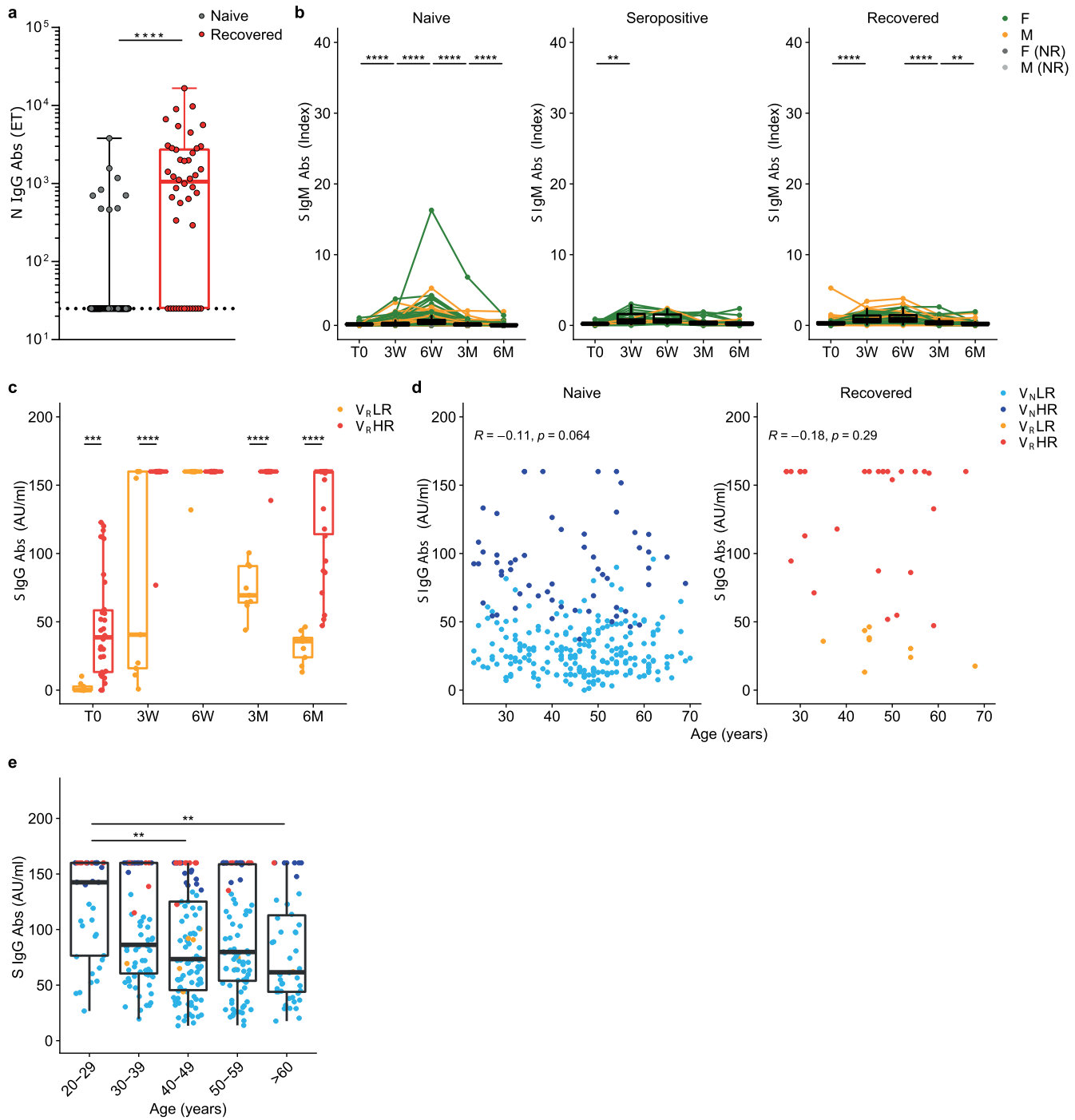

Extended Data Fig. 1 | Longitudinal analysis of humoral responses to BNT162b2 mRNA vaccine. a, ELISA showing N^{WT} antibody titers of SARS-CoV-2 naïve (n = 331) and SARS-CoV-2 recovered V (n = 48) subjects measured at T0. All data are shown as ELISA ETs based on a standard. The dotted line indicates LOD. **b**, CLIA analysis showing S^{WT} IgM titers in naive, seropositive and recovered subjects at T0, weeks 3 and 6 and months 3 and 6.NR subjects are also reported.**c**, CLIA analysis showing S^{WT} IgG titers in V_R subjects divided in V_RLRs and V_RHRs at T0, weeks 3 and 6 and months 3 and 6. **d**, CLIA analysis showing S^{WT} IgG titers in V_N (LRs and HRs) and V_R (V_RLRs and V_RHRs) subjects at month 6 vs subjects' age. **e**, CLIA analysis showing S^{WT} IgG titers in V_N (V_NLR and V_NHR) and V_R (V_RLR and V_RHR) subjects at month 6 grouped by age range. The same subjects were longitudinally analyzed. Boxes show median, upper and lower quartiles, and whiskers show 1.5x the interquartile range (IQR) on either side (panels b,c,e) or minimum/maximum (panel a). Each dot represents one subject. Each dot of box plots represents the average between two technical replicates of the same subject. All data are pooled. Statistics were calculated using two-sided Wilcoxon rank-sum test (panels **a**,**c**,**e**) or signed-rank test (panel **b**), with Benjamini Hochberg correction for multiple testing. **P ≤ 0.01; ***P ≤ 0.001; ****P ≤ 0.0001.

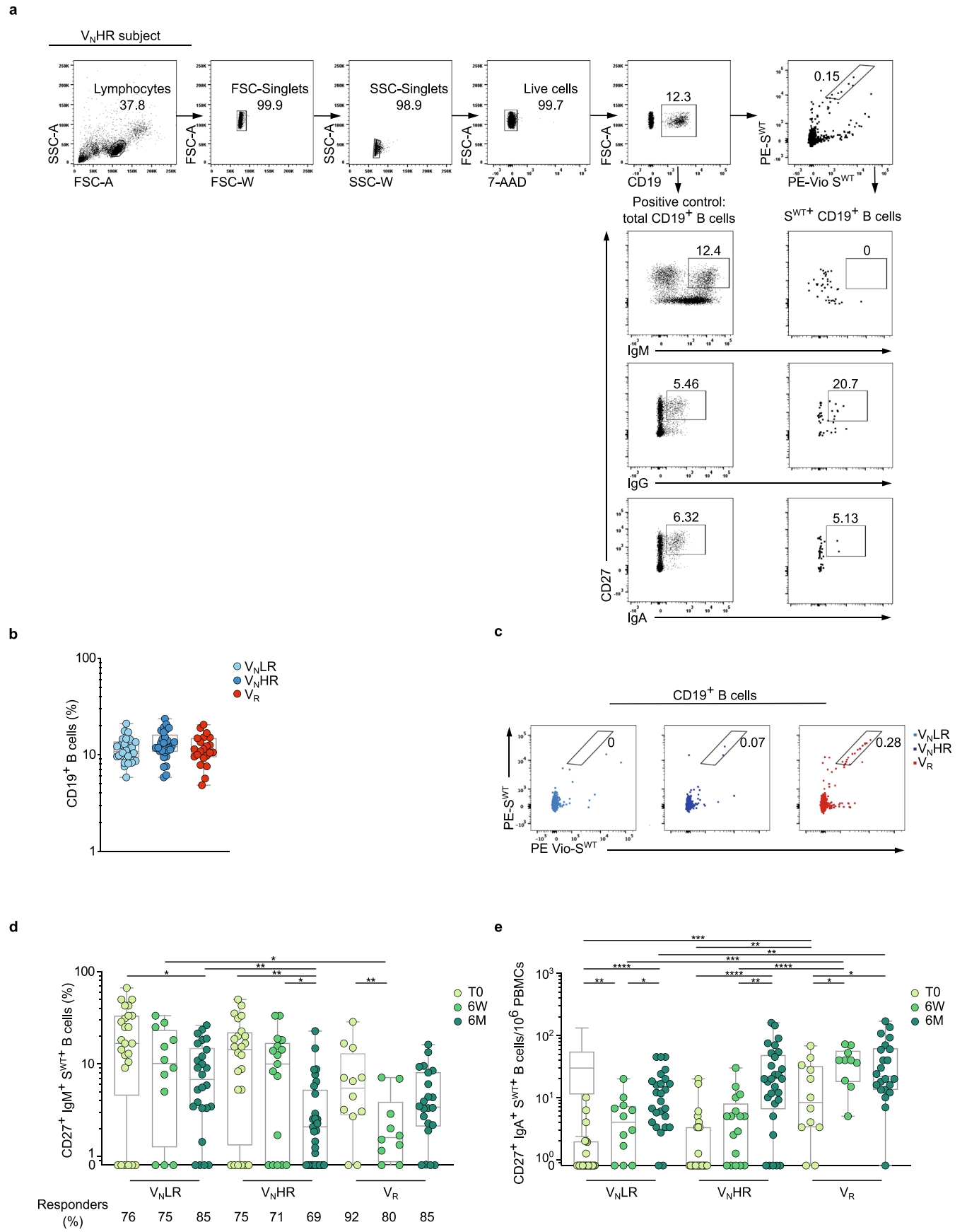

Extended Data Fig. 2 | See next page for caption.

Extended Data Fig. 2 | Analysis of B cell responses to SARS-CoV-2 BNT162b2 mRNA vaccine. a, Gating strategy ancestry: lymphocytes (FSC-A/SSC-A), FSC singlets (FSC-W/FSC-A), SSC singlets (SSC-W/SSC-A), live cells (PerCp^{-}Cy5.5-7-AAD/FSC-A), CD19^{+} cells (APC-Cy7-CD19/FSC-A), S^{WT} cells (PE-Vio-S^{WT} tetramer/PE-S^{WT} tetramer). IgM vs CD27 (APC-IgM/FITC-CD27), IgG vs CD27 (BV421-IgG/FITC-CD27), IgA vs CD27 (BV510-IgA/FITC-CD27) on gated CD19^{+} cells (positive control) and on gated S^{WT+} CD19^{+} B cells. **b**, Flow cytometry analysis showing the percentage of CD19^{+} B cells in V_NLR, V_NHR and V_R subjects at month 6. **c**, Representative flow cytometry dot plots of S^{WT}-specific tetramer^{+} CD19^{+}B cells from V_NLR, V_NHR and V_R subjects at T0. **d**, Flow cytometry analysis showing the percentage of CD27^{+} IgM^{+} S^{WT}- tetramer^{+} B cells in V_NLR, V_NHR and V_R subjects at T0, week 6 and month 6. Below: percentages of V_NLR, V_NHR and V_R subjects with active responses > 0.01. **e**, Flow cytometry analysis showing the cell number of CD27^{+} IgA^{+} S^{WT}- tetramer^{+} B cells per 10^6 PBMCs in V_NLR, V_NHR and V_R subjects at T0, week 6 and month 6. At T0: V_NLR (n = 25), V_NHR (n = 24), V_R subjects (n = 12). At week 6: V_NLR (n = 12), V_NHR (n = 17), V_R subjects (n = 10). At month 6: V_NLR (n = 26), V_NHR (n = 29), V_R subjects (n = 22). The same subjects were longitudinally analyzed. Box plots indicate median, interquartile range and minimum/maximum. Each dot of box plots represents the average between three technical replicates of the same subject. All data are pooled from multiple experiments. The dashed black line indicates LOD. Statistics were calculated using two-sided Wilcoxon rank-sum tests. *P < 0.05; **P < 0.01; ***P < 0.001; ****P < 0.0001.

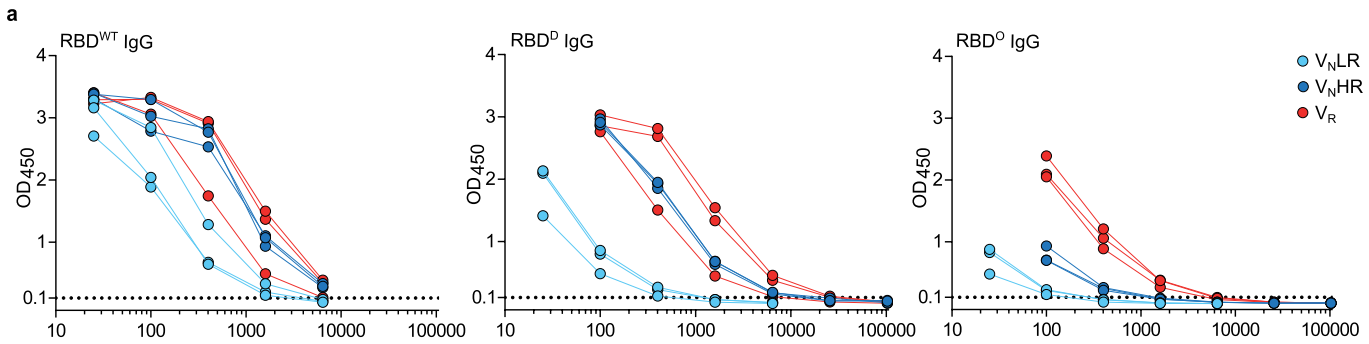

Extended Data Fig. 3 | Analysis of anti S-RBD^{WT} -RBD^{D} and -RBD^{O} binding Abs. a,ELISA titration analysis showing S-RBD^{WT}, -RBD^{D} and -RBD^{O} IgG from representative V_NLRs (n = 3), V_NHRs (n = 3), and V_R subjects (n = 3) at month 3. For S-RBD^{WT} IgG, plasma was diluted starting with 1:25 dilution, followed by 1:4 serial dilutions for all subjects. For S-RBD^{D} and S-RBD^{O} IgG, plasma was diluted starting with 1:25 dilution followed by 1:4 serial dilutions for V_NLRs or starting with 1:100 dilution followed by 1:4 serial dilutions forV_NHRs and V_R subjects.

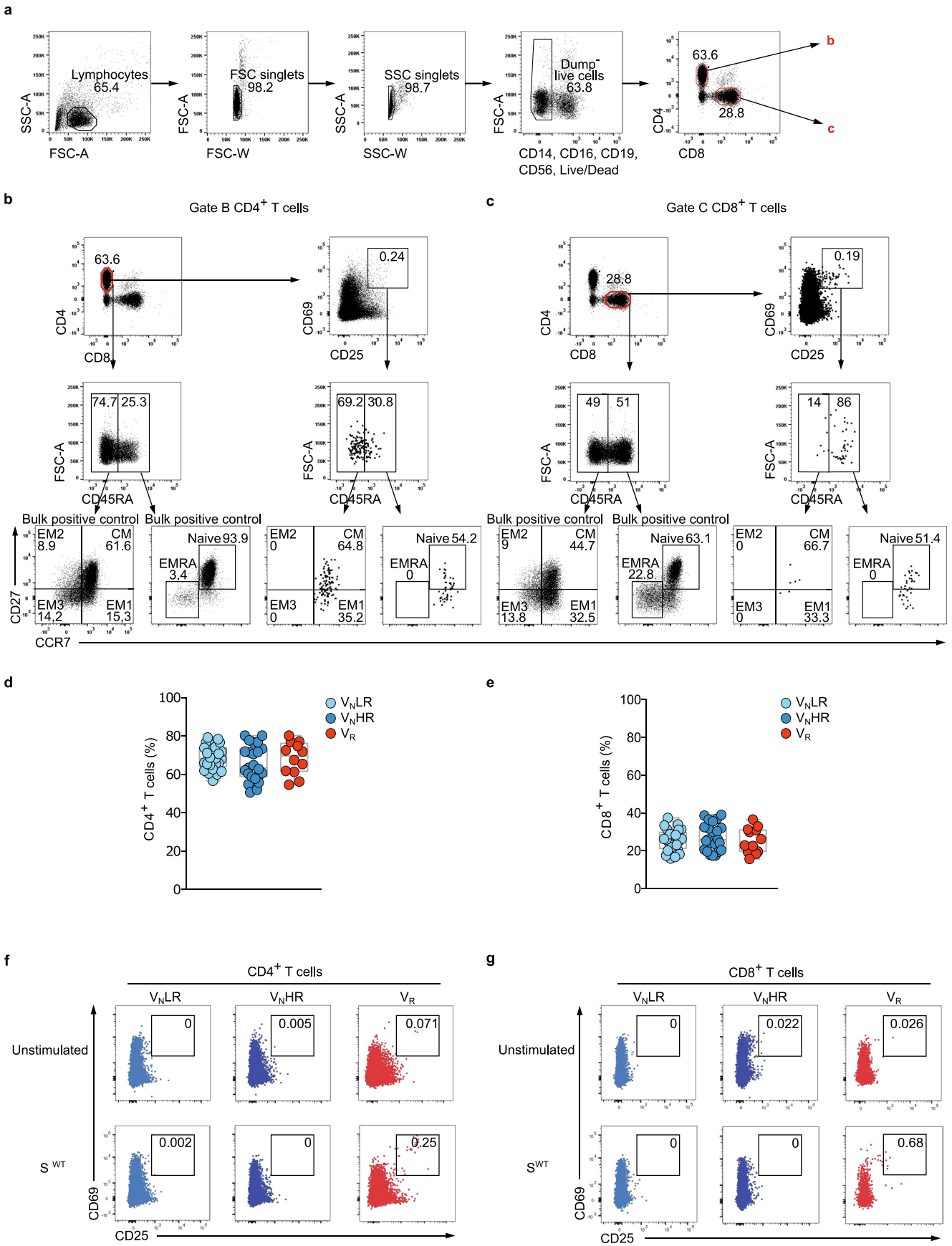

Extended Data Fig. 4 | See next page for caption.

Extended Data Fig. 4 | Flow cytometry gating strategy. a,Gating strategy ancestry: lymphocytes (FSC-A/SSC-A), FSC singlets (FSC-W/FSC-A), SSC singlets (SSC-W/SSC-A), Dump$^-$ live cells [Dead FVS450$^+$ cells and CD14$^+$ CD16$^+$ CD19$^+$ CD56$^+$ (Dump$^+$) cells excluded], CD4 vs CD8 (BV605-CD8/ BV786-CD4). **b, c**, Differentiation markers on CD4$^+$ (**b)** or CD8$^+$ (**c)**T cells. CD4$^+$ or CD8$^+$ T cells, CD25 vs CD69 (BV-510-CD25/APC-R700-CD69). CD4$^+$ or CD8$^+$ T cells with high gMFI levels for both CD25 and CD69 were gated as double positive cells. CD45RA (APC-CD45RA/FSC-A) on gated CD4$^+$ or CD8$^+$ and on gated CD25$^+$ CD69$^+$ CD4$^+$ or CD8$^+$ T cells, CCR7 vs CD27 (BV711-CCR7/ APC-H7-CD27) on gated CD45RA$^-$ and on gated CD45RA$^+$ cells. **d, e**, Flow cytometry analysis showing the percentage of CD4$^+$ (**d**) and CD8$^+$ (**e**) T cells in V_NLRs (n = 25), V_NHRs (n = 24), and V_R subjects (n = 12) at month 6. **f, g**, Representative flow cytometry dot plots of CD25 vs CD69 cells on gated CD4$^+$ (**f**) and CD8$^+$ (**g**) T cells from V_NLRs, V_NHRs and V_R subjects at T0, after 24h incubation with Medium (Unstimulated) or S^{WT}. Data are represented with background subtraction from paired unstimulated controls. The same subjects were longitudinally analyzed. Box plots indicate median, interquartile range, and minimum/maximum. Each dot of box plots represents the average between three technical replicates of the same subject. All data are pooled from multiple experiments. Statistics were calculated using two-sided Wilcoxon rank-sum tests.

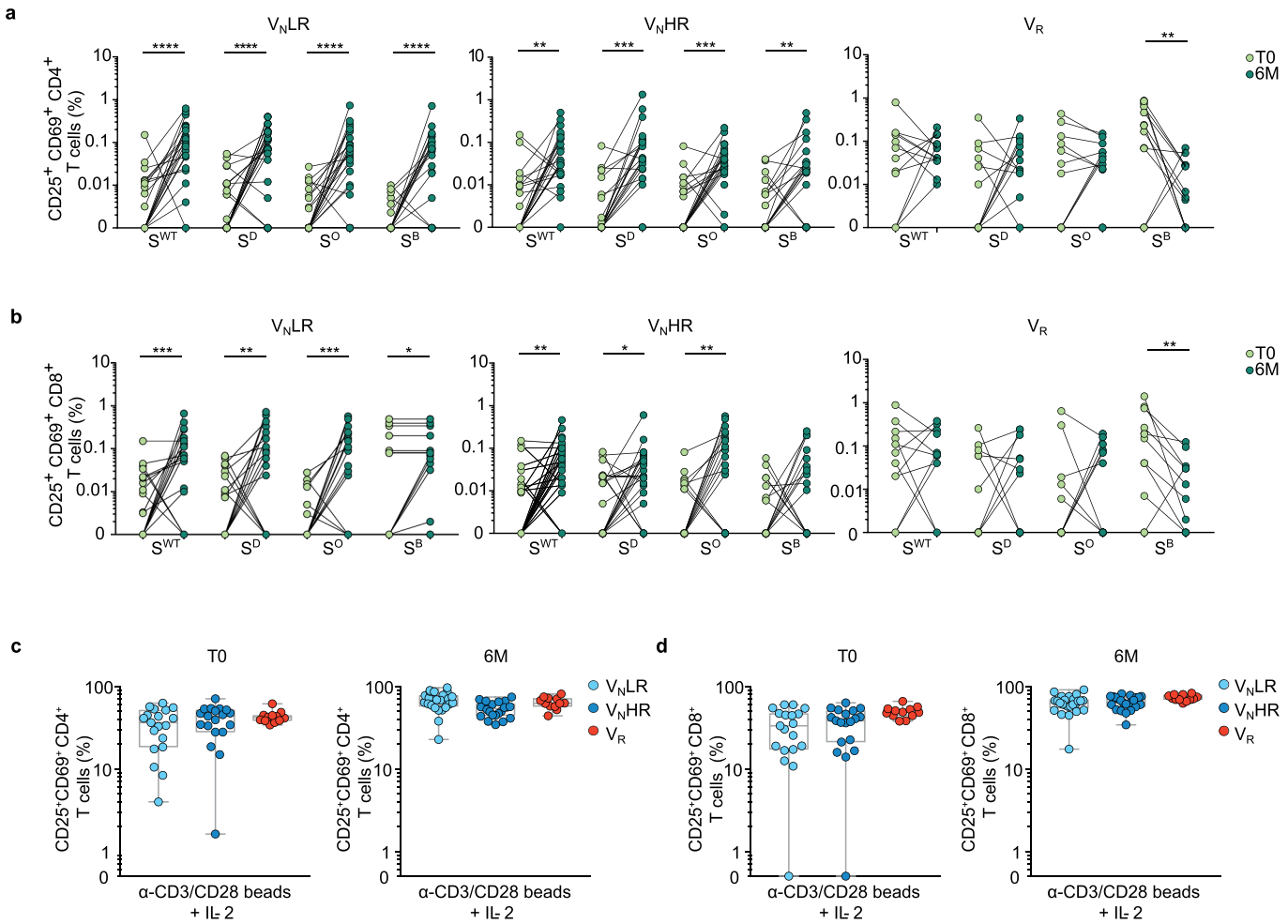

Extended Data Fig. 5 | Analysis of specific CD4⁺ and CD8⁺ T cell responses against S^{WT}, S^D, S^O and S^B in V_NLR, V_NHR and V_R subjects. a, **b**, Flow cytometry analysis showing the percentage of $CD25^+$ $CD69^+$ $CD4^+$ (**a**) and $CD25^+$ $CD69^+$ $CD8^+$ (**b**) T cells in V_NLRs (n = 25), V_NHRs (n = 24), and V_R subjects (n = 12) at T0 and month 6, after 24h incubation with S^{WT}, S^D, S^O or S^B peptide megapools. **c**,**d**, Flow cytometry analysis showing the percentage of $CD25^+$ $CD69^+$ $CD4^+$ (**c**) and $CD25^+$ $CD69^+$ $CD8^+$ (**d**) T cells from V_NLRs (n = 25), V_NHRs (n = 24), and V_R subjects (n = 12) at T0 and month 6, after 24h incubation with anti (α) -CD3 plus CD28 beads and IL-2. Data are represented with background subtraction from paired unstimulated controls. The same subjects were longitudinally analyzed. Each dot of box plots represents the average between three technical replicates of the same subject. All data are pooled from multiple experiments. Statistics were calculated using two-sided Wilcoxon signed-rank tests. *P < 0.05; **P < 0.01; ***P < 0.001; ****P < 0.0001.

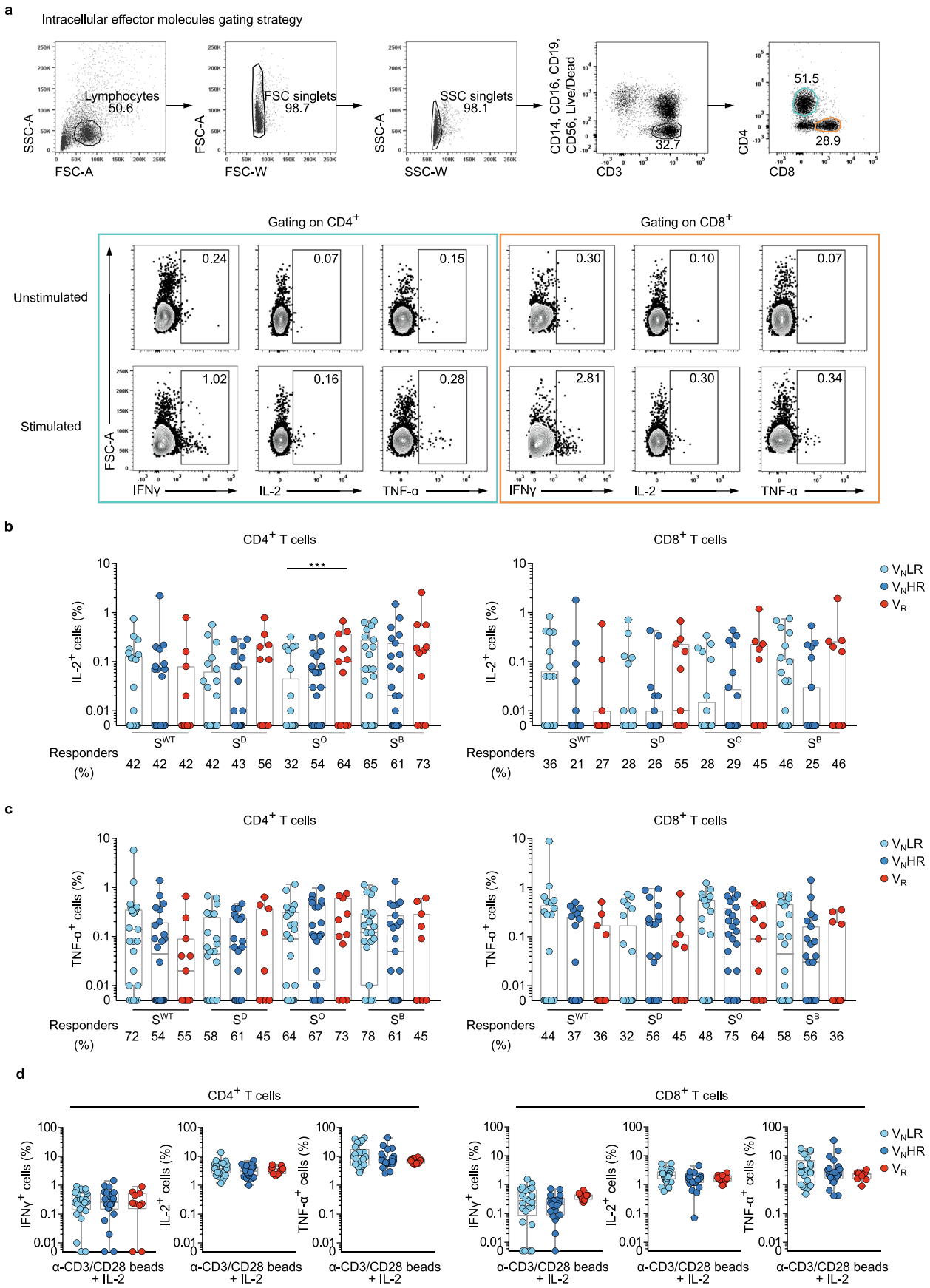

Extended Data Fig. 6 | See next page for caption.

Extended Data Fig. 6 | Analysis of effector molecules against S^{WT}, S^{D}, S^{O} and S^{B} in V_NLR, V_NHR and V_R subjects. a, Gating strategy ancestry: lymphocytes (FSC-A/SSC-A), FSC singlets (FSC-W/FSC-A), SSC singlets (SSC-W/SSC-A), $CD3^+$ $Dump^-$ live cells (BUV805-CD3/BV421-Dump) [Dead $FVS450^+$ cells and $CD14^+$ $CD16^+$ $CD19^+$ $CD56^+$ ($Dump^+$) cells excluded], CD4 vs CD8 (BV605-CD8/BV786-CD4). Intracellular effector molecules: IFN-γ (Pe-Cy7-IFN-γ/FSC-A), IL-2 (PE-IL-2/FSC-A) and TNF-α (PerCP-Cy5.5-TNFα-/FSC-A) on gated $CD4^+$ and on gated $CD8^+$ T cells. **b**, **c**, Flow cytometry analysis showing the percentage of IL-2^+ (**b**) and TNF-α^+ (**c**) cells on gated $CD4^+$ and $CD8^+$ T cells in V_NLRs (n = 25), V_NHRs (n = 24), and V_R subjects (n = 12) subjects at month 6, after 14h incubation with S^{WT},S^{D}, S^{O} or S^{B} peptide megapools. Below: percentages of subjects with active responses > 0.01. **d**, Flow cytometry analysis showing the percentage of IFN-γ^+, IL-2^+ and TNF-α^+ cells on gated $CD4^+$ and $CD8^+$ T cells from V_NLRs (n = 25), V_NHRs (n = 24), and V_R subjects (n = 12) subjects at month 6, after 14h incubation with α -CD3 plus -CD28 beads and IL-2. Data are represented with background subtraction from paired unstimulated controls. The same subjects were longitudinally analyzed. Box plots indicate median, interquartile range, and minimum/maximum. Each dot of box plots represents the average between three technical replicates of the same subject. All data are pooled from multiple experiments. Statistics were calculated using two-sided Wilcoxon rank-sum tests. ***P < 0.001.

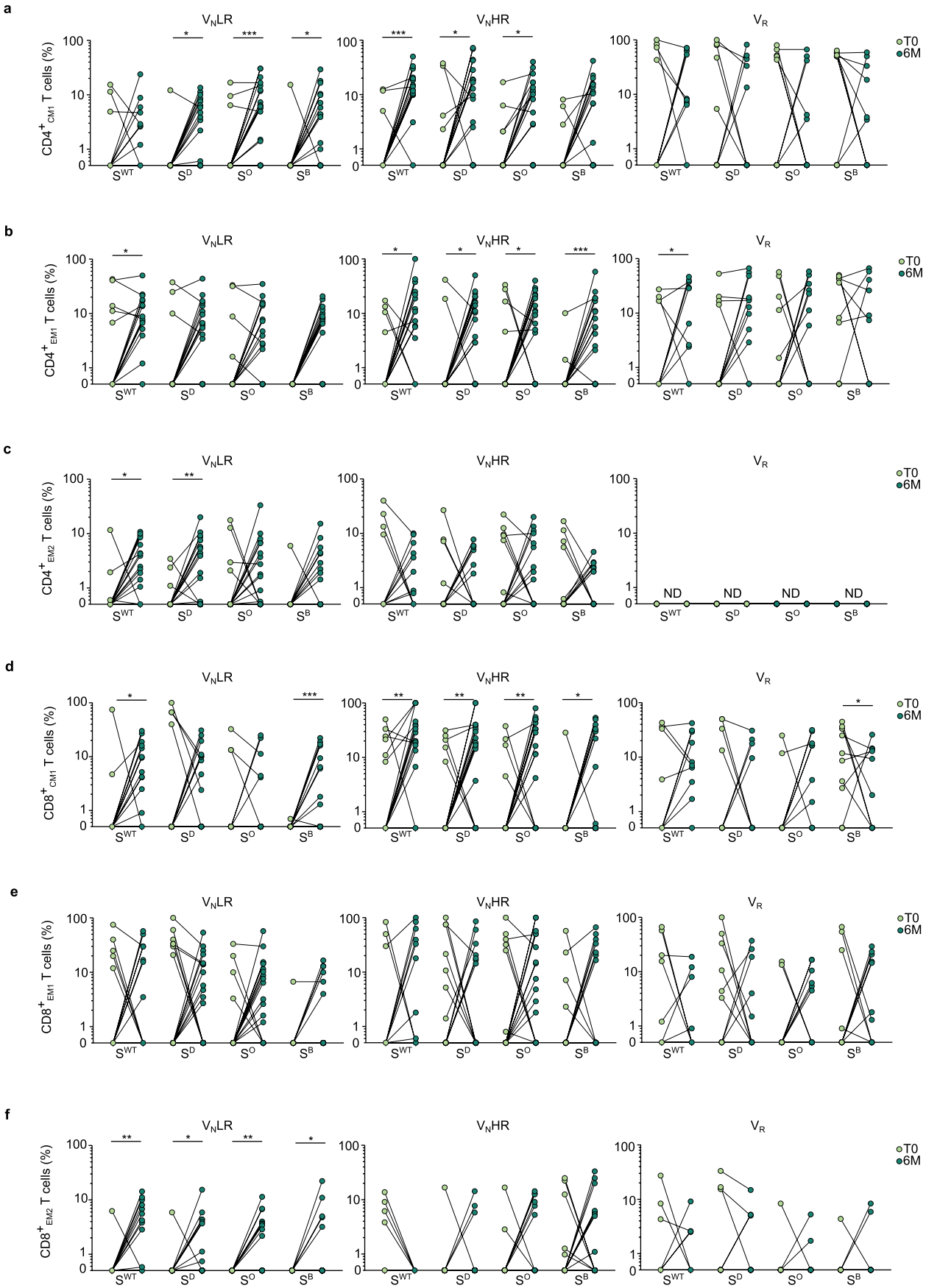

Extended Data Fig. 7 | See next page for caption.

Extended Data Fig. 7 | Analysis of specific CD4$^+$ and CD8$^+$ T cell responses against S^{WT}, S^D, S^O and S^B in V_NLR, V_NHR and V_R subjects. a-f, Flow cytometry analysis showing the percentage of CD25$^+$ CD69$^+$ CD4$^+$ T_{CM1} (**a**), T_{EM1} (**b**), T_{EM2} (**c**) cells and CD25$^+$ CD69$^+$ CD8$^+$ T_{CM1} (**d**), T_{EM1} (**e**), T_{EM2} (**f**) cells in V_NLRs (n = 25), V_NHRs (n = 24), and V_R subjects (n = 12) at T0 and month 6, after 24h incubation with S^{WT}, S^D, S^O or S^B peptide megapools. Data are represented with background subtraction from paired unstimulated controls. The same subjects were longitudinally analyzed. Each dot of box plots represents the average between three technical replicates of the same subject. All data are pooled from multiple experiments. Statistics were calculated using two-sided Wilcoxon signed-rank tests. *P < 0.05; **P < 0.01; ***P < 0.001; ND = not detected.

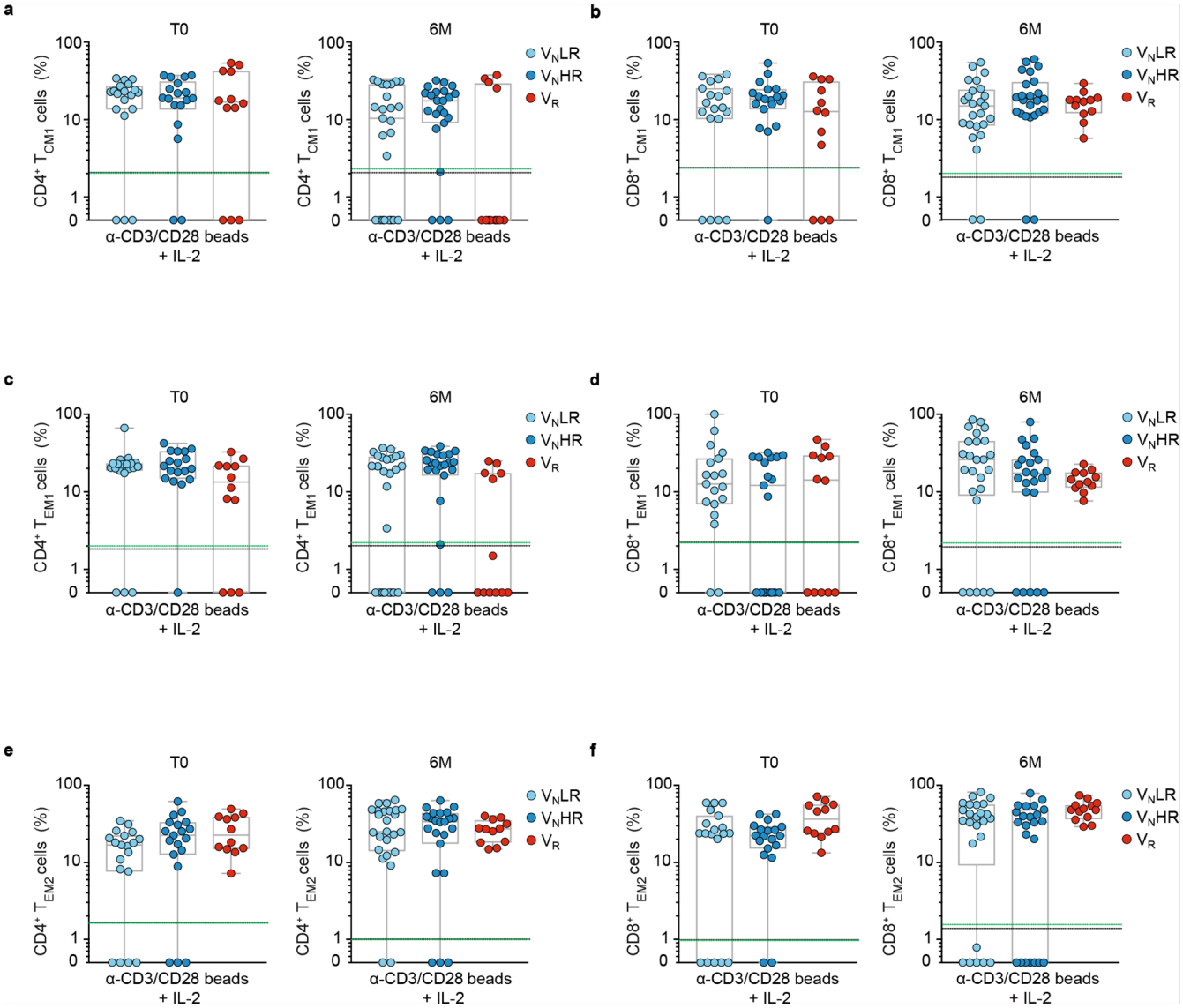

Extended Data Fig. 8 | Polyreactive CD4⁺ and CD8⁺ T cell responses in V_NLR, V_NHR and V_R subjects. a-f, Flow cytometry analysis showing the percentage of CD25⁺CD69⁺ T_{CM1} (**a**, **b**) T_{EM1} (**c**, **d**) and T_{EM2} (**e**, **f**) cells on gated CD4⁺ (**a**, **c**, **e**) and CD8⁺ (**b**, **d**, **f**) T cells from V_NLRs (n = 25), V_NHRs (n = 24), and V_R subjects (n = 12) at T0 and month 6, after 24h incubation with α-CD3 plus -CD28 beads and IL-2. The dotted black lines indicate the LOD. The dotted green lines indicate the LOS. The same subjects were longitudinally analyzed. Data are represented with background subtraction from paired unstimulated controls. Box plots indicate median, interquartile range, and minimum/maximum. Each dot of box plots represents the average between three technical replicates of the same subject. All data are pooled from multiple experiments. Statistics were calculated using two-sided Wilcoxon rank-sum tests.

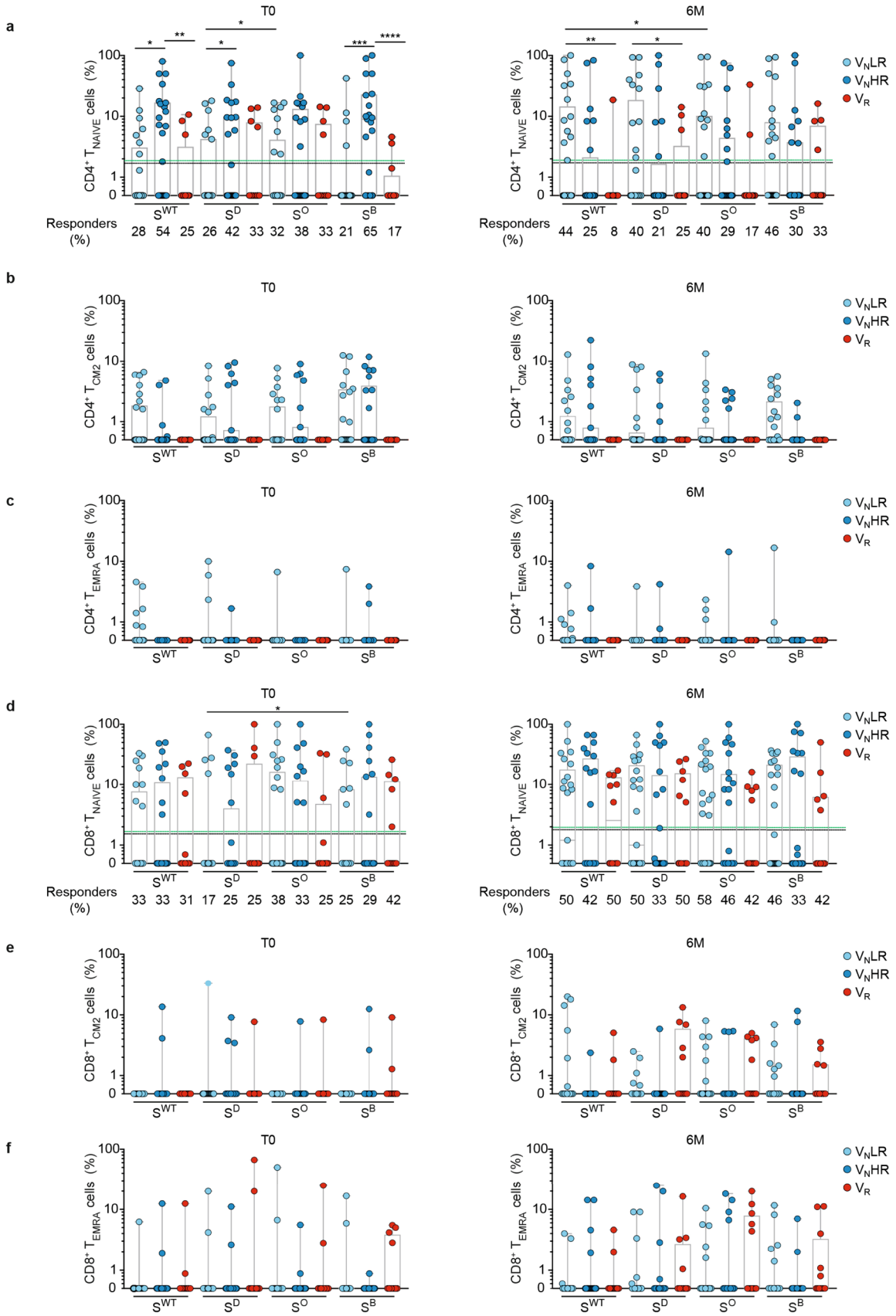

Extended Data Fig. 9 | See next page for caption.

Extended Data Fig. 9 | Analysis of S-specific T_N, T_{CM2}, and T_{EMRA} cell responses on gated $CD25^+$ $CD69^+$ $CD4^+$ and $CD8^+$ T cells. a-f, Flow cytometry analysis showing the percentage of T_N (**a, d**), T_{CM2} (**b, e**) and T_{EMRA} (**c, f**) cells on gated $CD25^+$ $CD69^+$ $CD4^+$ (**a**-**c**) and $CD8^+$ (**d**-**f**) T cells from V_NLRs (n = 25), V_NHRs (n = 24), and V_R subjects (n = 12) at T0 and month 6, after 24h incubation with S^{WT},S^D, S^O or S^B peptide megapools. The dotted black lines indicate the LOD. The dotted green lines indicate the LOS. Below: percentages of subjects with active responses > 0.01. Data are represented with background subtraction from paired unstimulated controls. The same subjects were longitudinally analyzed. Box plots indicate median, interquartile range, and minimum/maximum. Each dot of box plots represents the average between three technical replicates of the same subject. All data are pooled from multiple experiments. Statistics were calculated using two-sided Wilcoxon rank-sum tests. *P < 0.05; **P < 0.01; ***P < 0.001; ****P < 0.0001.

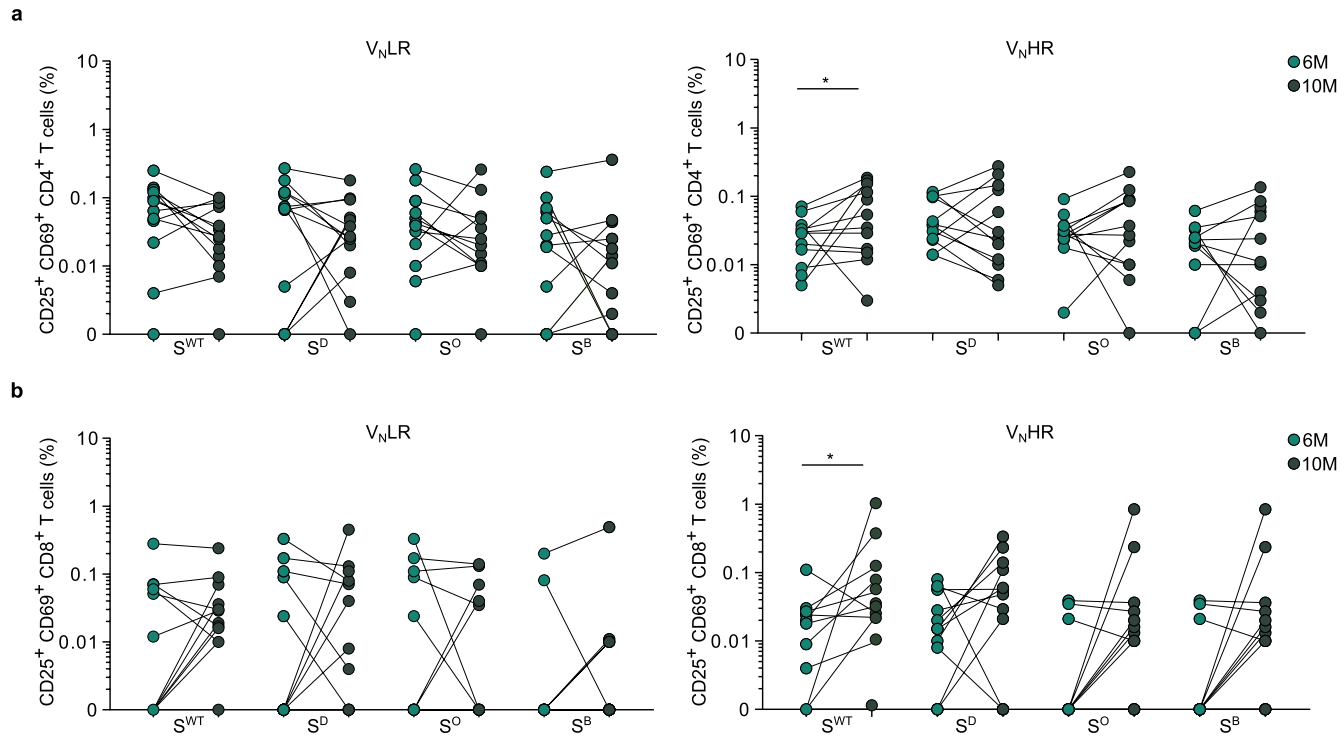

Extended Data Fig. 10 | Analysis of specific CD4⁺ and CD8⁺ T cell responses against S^{WT}, S^D, S^O and S^B in V_NLR, V_NHR and V_R subjects, at months 6 and 10 postvaccination. a, **b**, Flow cytometry analysis showing the percentage of $CD25^+$ $CD69^+$ $CD4^+$ (**a**) and $CD8^+$ (**b**) T cells in V_NLRs (n = 13), and V_NHRs (n = 12) at months 6 and 10, after 24h incubation with S^{WT}, S^D, S^O or S^B peptide megapools. The same subjects were longitudinally analyzed. Data are represented with background subtraction from paired unstimulated controls. Each dot of box plots represents the average between three technical replicates of the same subject. All data are pooled from multiple experiments. Statistics were calculated using two-sided Wilcoxon signed-rank tests. *$P < 0.05$.

nature portfolio

Corresponding author(s): Luigia Pace

Last updated by author(s): Aug 9, 2022

Reporting Summary

Nature Portfolio wishes to improve the reproducibility of the work that we publish. This form provides structure for consistency and transparency in reporting. For further information on Nature Portfolio policies, see our Editorial Policies and the Editorial Policy Checklist.

Statistics

For all statistical analyses, confirm that the following items are present in the figure legend, table legend, main text, or Methods section.

n/a	Confirmed	
☐	☒	The exact sample size (*n*) for each experimental group/condition, given as a discrete number and unit of measurement
☐	☒	A statement on whether measurements were taken from distinct samples or whether the same sample was measured repeatedly
☐	☒	The statistical test(s) used AND whether they are one- or two-sided *Only common tests should be described solely by name; describe more complex techniques in the Methods section.*
☒	☐	A description of all covariates tested
☐	☒	A description of any assumptions or corrections, such as tests of normality and adjustment for multiple comparisons
☐	☒	A full description of the statistical parameters including central tendency (e.g. means) or other basic estimates (e.g. regression coefficient) AND variation (e.g. standard deviation) or associated estimates of uncertainty (e.g. confidence intervals)
☐	☒	For null hypothesis testing, the test statistic (e.g. *F*, *t*, *r*) with confidence intervals, effect sizes, degrees of freedom and *P* value noted *Give P values as exact values whenever suitable.*
☒	☐	For Bayesian analysis, information on the choice of priors and Markov chain Monte Carlo settings
☒	☐	For hierarchical and complex designs, identification of the appropriate level for tests and full reporting of outcomes
☐	☒	Estimates of effect sizes (e.g. Cohen's *d*, Pearson's *r*), indicating how they were calculated

Our web collection on statistics for biologists contains articles on many of the points above.

Software and code

Policy information about availability of computer code

Data collection	Ids immunodiagnostics (termogenetics) Package GUI v3 r42; BD FACS Diva 8.0.2.
Data analysis	Prism 9, Flow Jo 10.4.2, R 3.6.3

For manuscripts utilizing custom algorithms or software that are central to the research but not yet described in published literature, software must be made available to editors and reviewers. We strongly encourage code deposition in a community repository (e.g. GitHub). See the Nature Portfolio guidelines for submitting code & software for further information.

Data

Policy information about availability of data

All manuscripts must include a data availability statement. This statement should provide the following information, where applicable:

- Accession codes, unique identifiers, or web links for publicly available datasets
- A description of any restrictions on data availability
- For clinical datasets or third party data, please ensure that the statement adheres to our policy

All data are included in this manuscript.

Field-specific reporting

Please select the one below that is the best fit for your research. If you are not sure, read the appropriate sections before making your selection.

☒ Life sciences ☐ Behavioural & social sciences ☐ Ecological, evolutionary & environmental sciences

For a reference copy of the document with all sections, see nature.com/documents/nr-reporting-summary-flat.pdf

Life sciences study design

All studies must disclose on these points even when the disclosure is negative.

Sample size	The first aim of the study was to characterize the anti-spike antibody levels after mRNA vaccination against SARS-CoV-2 in a wide cohort of subjects. Giving the exploratory design of the study, the characteristics of the participants were not pre-establised. A number of selected individuals, representative of the whole cohort, was deeply investigated for further flowcytometric analysis. All informations are included in the manuscripts.
Data exclusions	No data points were excluded.
Replication	A cohort of 379 individuals (table S1) was analyzed for anti-spike and anti-nucleocapsid antibody responses before and after vaccination (for Spike). The number of subjects analysed by flowcytometry , ELISA, and neutralization assay are listed in the manuscript, details are presented in table S2. The results obtained for each individual are shown. For anti-spike and anti-nucleocapsid antibody responses each dot represent the media average of two replicates for each subject (Fig.1). For
Randomization	No randomization was used in this study, since we are comparing three well defined cohorts: high responders, low responders and subject previously infected (EX-COVID).
Blinding	Blinding was not done in this study. The groups were defined based on the infection history and serological level of anti-spike IgG.

Reporting for specific materials, systems and methods

We require information from authors about some types of materials, experimental systems and methods used in many studies. Here, indicate whether each material, system or method listed is relevant to your study. If you are not sure if a list item applies to your research, read the appropriate section before selecting a response.

Materials & experimental systems

n/a	Involved in the study
☐	☒ Antibodies
☐	☒ Eukaryotic cell lines
☒	☐ Palaeontology and archaeology
☒	☐ Animals and other organisms
☐	☒ Human research participants
☒	☐ Clinical data
☒	☐ Dual use research of concern

Methods

n/a	Involved in the study
☒	☐ ChIP-seq
☐	☒ Flow cytometry
☒	☐ MRI-based neuroimaging

Antibodies

Antibodies used

anti-CD3 (clone SK7), BV510, 740202, 1:200, BD OptiBuild
anti-CD8 (clone SK1), BV605, 564116, 1:600, BD Horizon
anti-CD14 (clone MϕP9), BV421, 563743, 1:200, BD Horizon
anti-CD16 (clone 3G8), BV421, 562878, 1:600, BD Horizon
anti-CD19 (clone HIB19), BV421, 562440, 1:600, BD Horizon
anti-CD25 (clone 2A3), BV510, 740198, 1:200, BD OptiBuild
anti-CD27 (clone M-T271), APC-H7, 560222, 1:50, BD Pharmingen
anti-CD45RA (clone HI100), APC, 550855, 1:50, BD Pharmingen
anti-CD45RO (UCHL-1), Pe-Cy7, 560608, 1:200, BD Pharmigen
anti-CD45RA (clone 5H9), FITC, 556626, 1:200, BD Pharmingen
anti-CD56 (clone NCAM16.2), BV421, 562751, 1:200, BD Horizon
anti-CD69 (clone FN50), APC-R700, 565154, 1:50, BD Horizon
anti-CD197 (clone 150503), BV711, 566602, 1:100, BD Horizon
anti-CD4 (clone RPA-T4), BV786, 740962, 1:400, BD OptiBuild
anti-IFNγ (clone B27), Pe-Cy7, 557643, 1:50, BD Pharmingen
anti-IL-2 (clone MQ1-17H12), PE, 560709, 1:100, BD Pharmingen
anti-Granzyme B (clone GB11), AlexaFluor647, 560212, 1:100, BD Pharmingen
anti-TNFα (clone MAb11), PerCP-Cy5.5, 560679, 1:100, BD Pharmingen

The dilutions are indicative, as each Ab Abatch has been tested by titration.
anti-IgG HRP Peroxidase, 555788, 1:3000, BD Pharmigen

Chemiluminescence immunoassay (CLIA) was performed with TGS COVID-19 Control Set (Technogenetics CVCLCSGM), TGS COVID-19 IgM (CVCL100M) and TGS COVID-19 IgG (CVCL100G) according to the manufacturer instructions to quantify IgM and IgG.

The analysis of SARS-CoV-2 antigen-specific B cells was performed using the SARS-CoV-2 B Cell Analysis Kit (Miltenyi)

Validation

All antibodies were obtained from commercial vendors. After the evaluation of the instructions provided by the manufacturers, all antibody batches have been titrated to define the appropriate concentration for PBMC lebelling, and compared with the corresponding isotype controls.

Eukaryotic cell lines

Policy information about cell lines

Cell line source(s)	Human HEK293-NT: System Bioscience LV900A-1; Human freestyle 293 (293-F): Thermofisher Scientific R79007
Authentication	Short Tandem Repeat profiling
Mycoplasma contamination	The cell line were tested for mycoplasma contamination and they were negative
Commonly misidentified lines (See ICLAC register)	The cell lines used are not misidentified

Human research participants

Policy information about studies involving human research participants

Population characteristics	The characteristics of the human research participants are described in table S1 and S2 of the manuscript.
Recruitment	All the employers of Candiolo Cancer Institute were recruited.
Ethics oversight	Written informed consent was obtained from all the subjects. The study was performed in accordance with the declaration of Helsinki, and approved by the FPO /CRC Candiolo istitutional ethical board, project MemoryCoVax, N. 022-FPO21.

Note that full information on the approval of the study protocol must also be provided in the manuscript.

Flow Cytometry

Plots

Confirm that:

☒ The axis labels state the marker and fluorochrome used (e.g. CD4-FITC).

☒ The axis scales are clearly visible. Include numbers along axes only for bottom left plot of group (a 'group' is an analysis of identical markers).

☒ All plots are contour plots with outliers or pseudocolor plots.

☒ A numerical value for number of cells or percentage (with statistics) is provided.

Methodology

Sample preparation	PBMCs were prepared, coltured and labeled according to standard protocol.
Instrument	BD Fortessa X20
Software	BD FACS Diva 8.0.2, FlowJo 10.4.2
Cell population abundance	N/A. No sorting was performed.
Gating strategy	The B cell gating strategy starts with Lymphocyte gate based on SSC-A vs FSC-A, then singlets were identified by FSC-A vs FSC-W,followed by SSC-A vs SSC-W. Live cells were identified with 7-AAD. B cell were identified by CD19 expression. Antigen-specific WT+B cells were identified using the combination of WT-tetramers. On Total B cells and on WT+CD19+B cells IgM, IgG and IgA expression were identified in combination with CD27. (Extended Data Figure 2). The T cell gating strategy starts with Lymphocyte gate based on SSC-A vs FSC-A, then singlets were identified by FSC-A vs FSC-W followed by SSC-A vs SSC-W. T live cells were identified with cell exclusion dyes as Live/Dead and DUMP channel composed by CD14,CD16,CD19,CD56, following T cell identification by expression of CD4 and CD8. In both CD4 and CD8 gates antigen-specific cells were identified using CD25 vs CD69 combination. On Total CD8 and CD4 and in the antigen-specific CD4+CD25 +CD69+ or CD8+CD25+CD69+gate,FSC-A vs CD45RA was performed. Memory subsets were identified with CCR7 vs CD27 expression on CD45RA+ and CD45RA- on Total CD4 and CD8 T cells and CD4+CD25+CD69+ or CD8+CD25+CD69+ T cells.

(Extended Data Figure 4).

☒ Tick this box to confirm that a figure exemplifying the gating strategy is provided in the Supplementary Information.